

General Disclaimer

One or more of the Following Statements may affect this Document

- This document has been reproduced from the best copy furnished by the organizational source. It is being released in the interest of making available as much information as possible.
- This document may contain data, which exceeds the sheet parameters. It was furnished in this condition by the organizational source and is the best copy available.
- This document may contain tone-on-tone or color graphs, charts and/or pictures, which have been reproduced in black and white.
- This document is paginated as submitted by the original source.
- Portions of this document are not fully legible due to the historical nature of some of the material. However, it is the best reproduction available from the original submission.

NGR-14-007-151

SQT

Use of Fröhlich- Raimes and Other
Electronic Models for Physical
Properties of Metals and Alloys.

James T. Waber

(NASA-CR-169001) USE OF FROEHLICH-RAIMES
AND OTHER ELECTRONIC MODELS FOR PHYSICAL
PROPERTIES OF METALS AND ALLOYS
(Northwestern Univ.) 74 P HC A04/MF A01

N82-25366

Unclas
CSCL 11F G3/26 22707



USE OF FRÖHLICH-RAIMES AND OTHER ELECTRONIC MODELS
FOR PHYSICAL PROPERTIES OF METALS AND ALLOYS*

James T. Waber †

The effectiveness of the Fröhlich-Raimes model in treating force constants and alloy behavior is discussed. Typical predictions of trends which have been made are: of the deviation of Vegard's Law and the variation of the bulk modulus with pressure and with alloying elements. The simple model of Koskimaki and Waber using the linear combination of the density of states has lead to several useful predictions for titanium-based alloys. This model will be discussed and recent results are reviewed.

* This research was supported in part by the National Aeronautics and Space Administration and by the U. S. Atomic Energy Commission. The work was initiated while the author was at Los Alamos Scientific Laboratory.

† Department of Materials Science, Northwestern University, Evanston, Il. 60201

Waber

Several years ago Brooks¹ and Wigner and Seitz² took up an investigation on the effectiveness of a volume-dependent theory of metals originally developed by Fröhlich³ in 1937 and modified by Raimes^{4,5} to include several conduction electrons per atom. In an unpublished thesis, Bernstein⁶ applied this Fröhlich-Raimes (FR) method to rare earth metals. Brooks notes that the equilibrium lattice spacing in normal metals is essentially determined by pressure of the Fermi gas of free electrons.

In 1961, Larson and Waber⁷ reinvestigated the problem and noted an undetected asymptotic singularity existed in the basic equation. When this was removed by retaining more terms before truncation of a series expansion for the wave function, better agreement with experimental data was obtained.

Another modification by Waber, Larson and Smith⁸ was to derive the equations assuming that the state at the bottom of the conduction band could have an angular momentum greater than $\ell=0$. This permitted them to investigate transition metals. A brief review of the theory and some results will be given below before applying it to alloys, since the recent developments have not been reported in the literature.

Before continuing with that topic, it is desirable to give a little background on the second model which will be used inasmuch as it is apparently unknown except to a small circle of colleagues. In the case of metals, the Pauli exclusion principle requires that a distinct set of quantum numbers be assigned for each conduction electron coming from an atom in the solid. Instead of the usual set of n, ℓ, m and spin for free atoms, they

are k_x , k_y , k_z and spin, and are associated with the momentum \underline{k} of itinerant electrons. If the density of atoms per cubic centimeter becomes large enough, the discrete spectrum of energies associated with each \underline{k} value can be replaced by a piecewise continuous $E(\underline{k})$ curve. The number of discrete states within any energy range E to $E+dE$ is replaced by the density of states function $N(E)$. The band structure of metals is concerned with calculating such $N(E)$ curves for a pure metal and with deducing various observable quantities from them.

When the original proponents of this theory, such as Jones⁹ and Hume-Rothery¹⁰ theory applied it to metallic alloys, they assumed a Rigid Band model (RB). Slater¹¹ made one of the first uses of this model to explain the variation of magnetism of alloys; the famous Slater-Pauling curve¹² was the result. These men were keenly aware of the limitations of the model, but insufficient information was available for them to regard it initially as anything but a working hypothesis. It has proved to be very successful in making important predictions during the last thirty-five years and many experimentalists have verified the essential features; the comments of Raimes¹³ are interesting. However, repeatedly small and sometimes large deviations from the Rigid Band prediction have been noted.

In an extensive series of band calculations for 3d transition metals, Waber and Snow¹⁴ showed that the band structure was far from rigid for such a series of metals; but they also showed why the Rigid Band (RB) model worked well. Despite changes in the shape and the location of the bands for individual metals, the plot of $N(E_F)$ at the Fermi level E_F when plotted against the atomic number had the two hump shape of the original $E(\underline{k})$ curve computed for pure metals by Manning¹⁵ and by Chodorow¹⁶.

Waber proposed that it would be preferable to use a linear

combination of the two (or three) density of states for the constituents in dealing with alloys. In discussions during the conference on the Electronic Density of States held at the Bureau of Standards, Waber used the LCDS model to estimate¹⁷ (a) densities of states curves which have three humps and (b) a typical curve of $N(E_F)$ versus composition for one type of titanium alloy. He also presented the three peak $N(E)$ curves for several 4d metals. Koskimaki and Waber¹⁸ have computed these for a number of alloy systems. Collings and Gegel¹⁹ have made effective use of the calculations recently. It is appropriate to present further the justification of this LCDS model and to record some of the results obtained with it. Independently, Sterns²⁰ studied a form of the LCDS model and concluded that E_F should be constant.

Let us contrast these two approaches to the behavior of alloys. They depend very directly on the average spatial density of electrons in the metal. The modifications of the Fröhlich-Raimes Theory ignore all questions about the arrangement of atoms in the solid. It is also assumed that the Fermi energy ($\hbar^2 k_F^2$) depends only on the number of electrons per atom (i.e., on the (e/a) ratio).

The LCDS theory is predicated on the detailed $E(k)$ curves for each constituent, which in turn is based on the local arrangement of atoms. That is, Snow and Waber¹⁴ have shown that the $E(k)$ curve is not the same for the BCC and FCC forms of the same metal.

Thus, the LCDS model is better able to cope with alloys and such phenomena as short range order and clustering, than is the volume dependent FR model. It in turn is more effective than the (e/a) dependent RB model. Each model has a range of problems for which it is effective. For the calculation of cohesive energy, compressibility, etc., the FR approximation will be very useful. For the behavior of the specific heat and magnetism

of alloys, the LCDS model will be a distinct improvement over the RB model. In principle, the volume (or pressure) dependence of $E(k)$ curves can be calculated by a band calculation such as by the APW method. Averill²¹ and independently Perrot²² have calculated the cohesive energy for alkali metals with considerable success. Very recently, Snow²³ has done it for copper. However, these were extensive calculations which consumed large amounts of time on the computer. It is not practical to do exploratory research on alloys by such methods.

The two approximations outlined in contrast are very simple to carry out and therefore lend themselves to treating complicated problems. It is with these justifications and limitations in mind that we undertake to study the behavior of alloys.

Formulation of Fröhlich-Raimes Model

The basic assumption is that the behavior of the conduction electrons in a metal closely approximates those confined to a sphere of radius R_S . Next one assumes that the ion core with its charge of Ne (or N , in the atomic units where $e = \hbar = m = 1$) does not occupy a significant fraction of the sphere. One solves the Schroedinger equation for one electron confined to the Wigner-Seitz sphere, which also contains an ion core. We will call $f_{\ell 0}(\lambda)$ the radial part of the wave function in this field (averaged over the 4π solid angle). The subscript zero indicated the ground state for the angular moment ℓ . The Schroedinger equation can be written as

$$\frac{df_{\ell 0}}{dr^2} + \frac{2}{r} \frac{df_{\ell 0}}{dr} + \left[E_0(R_S) - V_{\ell}(r^2) - \frac{\ell(\ell+1)}{r^2} \right] f_{\ell 0} = 0 \quad (1)$$

The usual Wigner-Seitz boundary condition²⁴ is applied, namely that the gradient vanishes

$$\left. \frac{df_{\ell 0}}{dr} \right|_{r=R_s} = 0 \quad (2)$$

In the space available, it is not practical to discuss the mathematical part of this problem. Only the results in the form of the principal equations will be indicated.

As Waber, Larson and Smith²⁵ show, the lowest eigen-value E_0 depends on R_s in the following simple way

$$E_0(R_s) = \frac{N}{R_s} \left(\frac{R_0^2}{R_s^2} - 3 \right) + \frac{3\ell(\ell+1)}{R_s^2} \left(1 - \frac{2R_0}{3R_s} \right) \quad (3)$$

The parameter R_0 corresponds the radius of which the energy becomes a minimum. At the other extreme end, when R_s becomes infinitely large, E_0 approaches I_n which is the n^{th} ionization potential for removing all but one of the valence electrons from the atom in question.

Let us call β^2 the positive energy difference between the free ion and the E_0 for the metallic case, and call the ionization potential w^2 . After substituting R_0 for R_s in Equation 3, we find that

$$\begin{aligned} \beta^2 &= -E_0(R_0) - I_N \quad (4) \\ &= \frac{2N}{R_0} - \frac{\ell(\ell+1)}{R_0^2} - w^2 \quad (4a) \end{aligned}$$

In the procedure outlined initially by Fröhlich, one expresses the eigen-function where

$$f_{l_0}(r) = \exp(-wr) r^P \sum_{k=0}^J C_k r^{-k} \quad (5)$$

in terms of a power series $P = n/w$.

The recursion formula for the coefficients in the power series can be shown to be

$$\frac{C_{k+1}}{C_k} = \frac{(P-k-1)(P-k-2) - l(l+1)}{-2w(k+1)} \quad (6)$$

Then one requires that the function be well behaved at the special value R_0 of the sphere boundary. Thus, as a generalization of the solution which Fröhlich and Raimes found, one can write

$$\frac{1}{f_{l_0}} \left(\frac{df_{l_0}}{dr} \right) \Big|_{r=R_0} = \frac{R_0(\beta-A) \cot \beta R_0 - (1+\beta R_0 A)}{R_0(1+Ar_0 \cot \beta R_0)} \quad (7)$$

where A is an arbitrary small constant (which it will be convenient to set to zero).²⁵

Substitution of the wave function alternatively leads to

$$\frac{d \ln f_{l_0}(r)}{dr} \Big|_{r=R_0} = \left\{ \frac{\sum_{k=0}^J (-k) C_k / r^{k+1}}{\sum_{k=0}^J C_k r^{-k}} \right\} \Big|_{r=R_0} \quad (8)$$

numerically by iteration.

By experience one need include at most six terms and in many cases two will suffice. These equations reduce to the ones given by Raimes when one sets $l=0$.

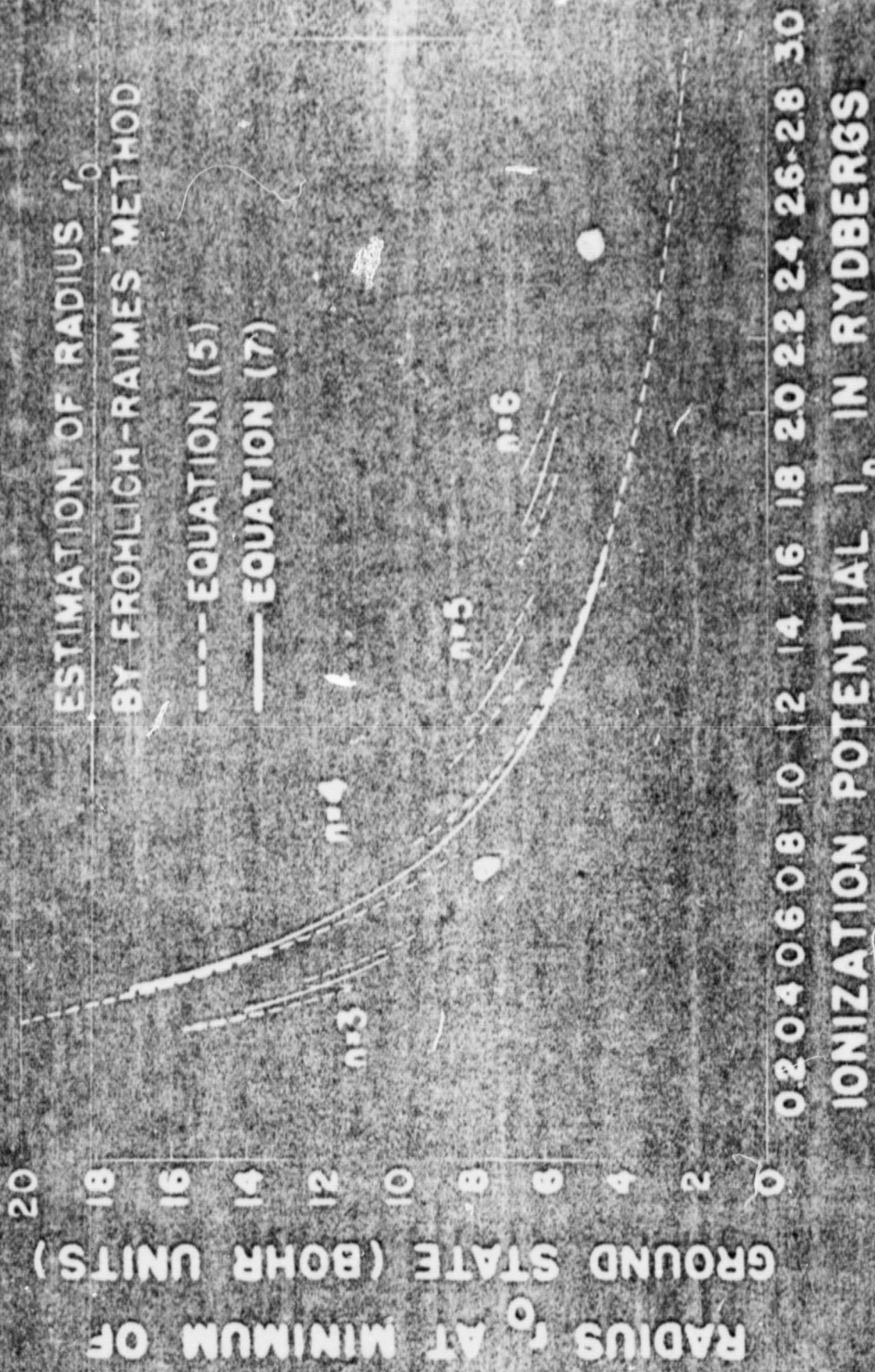
A plot of the ground state radius R_0 is presented in Fig. 1, as a function of I_4 . A discontinuity is found because the cotangent function approaches ($\pm \infty$) when its argument equals π . This behavior of the logarithmic derivative corresponds to f_{l0} vanishing at the cell boundary for a specific energy. If one desires, this difficulty can be eliminated by retaining the terms multiplied by A in the logarithmic derivative, as the smooth curves show. Insets for other values of N are shown.

The next step in this volume dependent theory is to put $n-1$ free electrons back into the spherical cell. There are several types of interactions between the electrons. The first is Coulomb energy of the N electrons. The second is the mean Fermi energy of these electrons confined to sphere of radius R_s . The third is the free electron exchange energy. A small correction is also included for correlation. Thus, the total energy for the N valence electrons is given by the simple formula

$$E(R_s) = E_0(R_s) + \frac{1.2N}{R_s} + \frac{2.21}{r_s^2} - \frac{0.916}{r_s} - E_{\text{corr}} \quad (9)$$

Inherent in this expression is the idea that $f_{l0}(r)$ is approximately constant throughout a significant fraction of the sphere (for cases Raimes⁴ studied, the fraction was approximately 90 percent.) In uniform electron gas, we can set r_s as the radius of the Fermi hole, namely $R_s/\sqrt[3]{N}$. The simplest form of correlation was used, namely that based on Wigner's approximation formula

$$E_{\text{corr}} = \frac{-0.288}{R_s + 5.1} \quad (10)$$



ORIGINAL PAGE
COLOR PHOTOGRAPH

ORIGINAL PAGE IS
OF POOR QUALITY

While improved treatments of exchange are available such as those by Slater and his colleagues²⁶ and by Liberman²⁷, significant precision should not be expected with this oversimplified model. Typical interaction terms which are independent of the element involved, are presented in Fig. 2 for $N=4$. While it might be desirable to employ an improved treatment of correlation done by Pines and Matveev²⁸, it is not likely to lead to significantly different results. Just as Slater has indicated in his recent studies that the exchange term should be multiplied by a constant α_s , one could correct the kinetic energy by dividing by the effective mass, m_e^* each of the coefficients might be regarded as adjustable parameters.

It has been decided to apply the more stringent test to the model, namely, the original free-electron coefficients have been used in this heuristic study.

The energies $E_o(R_s)$ and $E_T(R_s)$ are presented in Fig. 3 for titanium and zirconium. The equilibrium radius corresponding to a minimum in $E_T(R_s)$ is designated ρ . Even though the interaction energies depend only on N and are independent of the specific metal being studied, the curves of $E_o(R_s)$ may be different for two very similar metals as titanium and zirconium.

Estimation of Other Physical Quantities

Brooks¹ noted that the experimental cohesive energy per valence electron is surprisingly constant. For 23 elements it ranges from 0.060 for Cesium to 0.137 Rydbergs per atom for carbon.

The cohesive energy data tabulated for the lanthanides by Gschneidner²⁹ and the data of Trulson, Hudson and Spedding³⁰ for the heat of sublimation at 298°K were divided by the number

ORIGINAL PAGE IS
OF POOR QUALITY

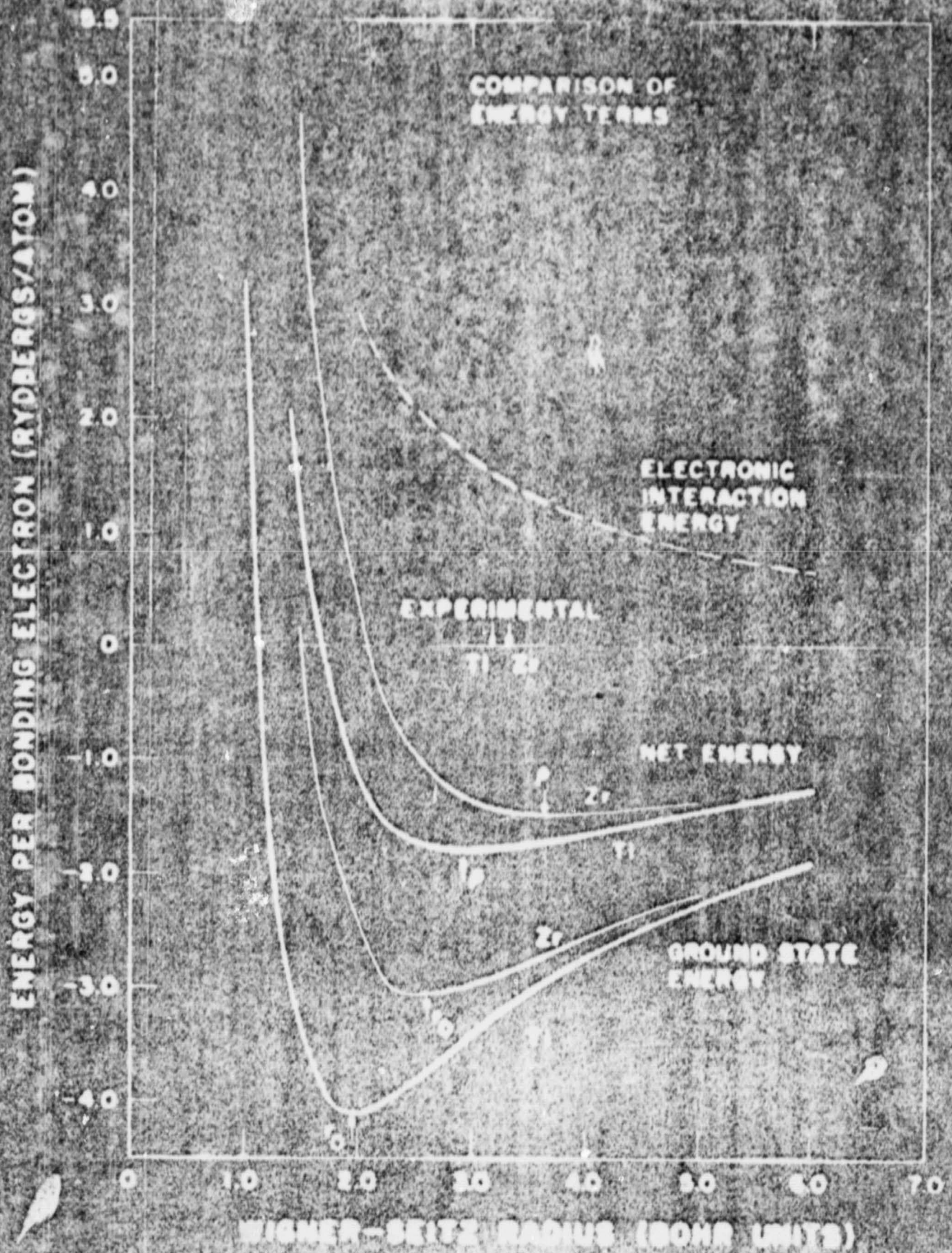
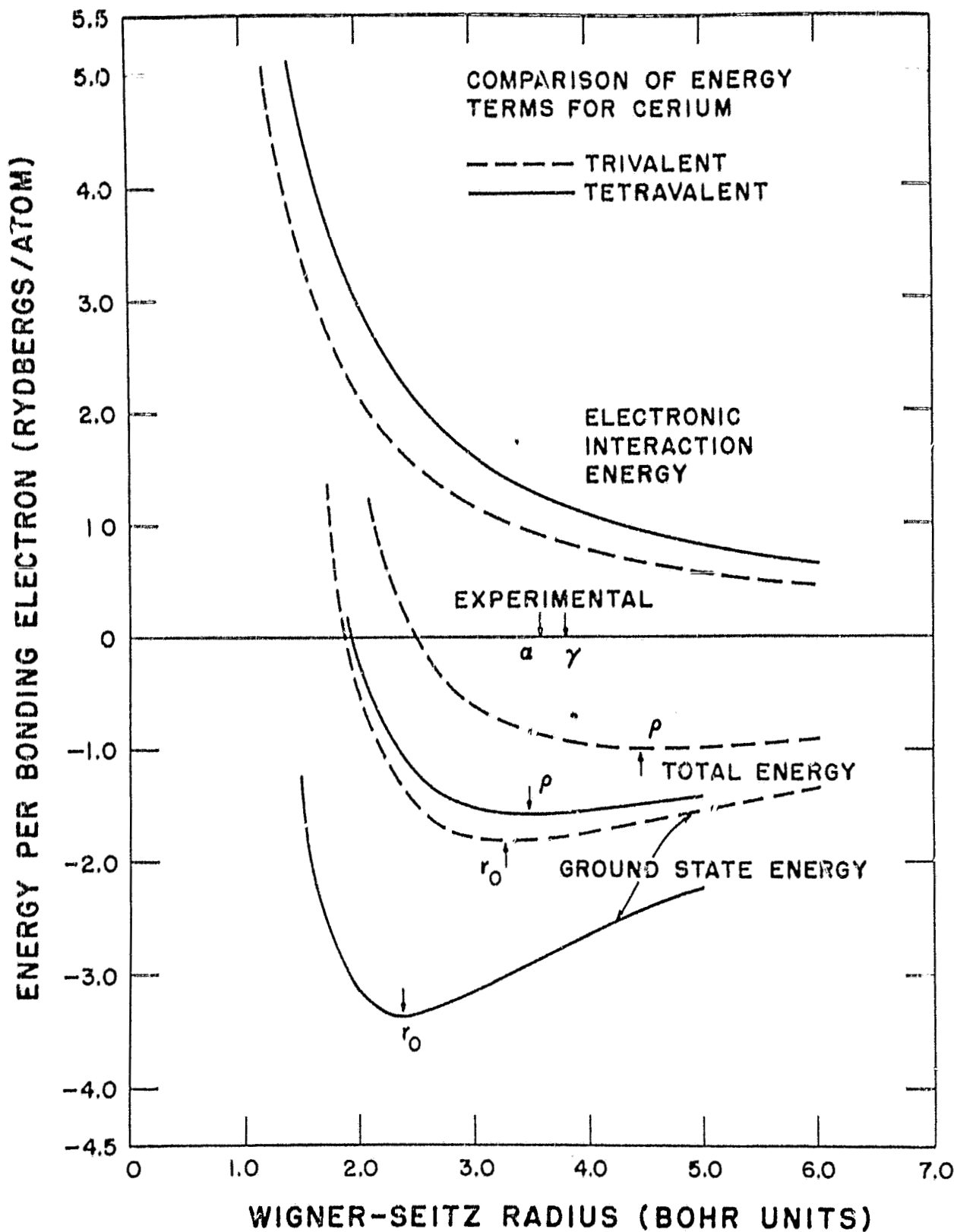


Fig. 3.
Determination of R_0 and ρ from E_0 and E_T curves
of titanium and zirconium



of valence electrons. This energy was found to vary for the lanthanides from 0.106 Rydberg for lanthanum and 0.0636 for thulium.

The cohesive energy S , i.e. the heat of sublimation of 0°K , can be obtained from the total energy at ρ by means of the expression,

$$S = \sum_j^n I_j - NE_T(\rho) \quad (11)$$

wherein the several ionization potentials I_j are summed.

The pressure-volume relation which leads to the compressibility χ at any pressure can be obtained in a straightforward manner from the $E_T(R_s)$ curve. Raimes⁴ points out that the pressure P corresponding to a relative change in volume can be obtained from the expressions

$$P = \frac{-N}{4\pi R_s^2} \left(\frac{dE_T}{dR_s} \right) \quad (12)$$

$$-\frac{\Delta V}{V} = 1 - \left(R_s/\rho \right)^3 \quad (13)$$

Note that 1 atomic unit of pressure used in (12) is equal to $150 \times 10^6 \text{ kg/cm}^2$. No attempt has been made here to correct these data to absolute zero although generally speaking this change would tend to improve the agreement between calculated and experimental values. The compressibility χ at zero pressure can be obtained from the second derivative of $E_T(R_s)$. With one exception, the listed values of the experimental compressibility were all taken from Bridgmen's tabulation³¹ of the quantity χ using the more recent data for 75°C . The value for silicon is from Pearson and Brattain³².

Experimental and calculated values of the three physical

constants ρ , S and χ are presented in Table I for a number of metals and semi-metals. In as much as S is the difference of two large terms, the effect of any error in estimating the individual electronic energies is greatly magnified. To partially overcome this objection, an experimental value of E_T was obtained by adding the several experimental ionization potentials $\sum I_j$ to the experimental heat of sublimation. These two values of $E_T(\rho)$ are included in the table. The energy conversion factor used was one Rydberg per atom equals 313.66 kcal/mole. The values of the heat of sublimation S for monatomic gaseous species and corrected to 298°K were taken from Teatum et al³³.

Wherever possible, the ionization potentials obtained by C. E. Moore-Sitterly³⁴ from spectroscopic data were used. One of the most readily usable and complete tabulations of ionization potentials has been presented by Finkelnburg and coworkers³⁵. The ionization potentials for Hf III and Hf IV were recently given by Klinkenberg, van Kleef and Noorman³⁶. The ionization potentials for thorium are not well known, the sum is probably accurate to better than 5 per cent.

Values of χ , S and ρ were obtained independently by Raimes³⁷ who used the simplified theory cited above⁴. For comparison, these values for trivalent and tetravalent metals are presented in Table II.

In the calculation by Bernstein⁶, of the cohesive energy of the lanthanides, the experimental values of the third ionization potential I_3 were used, where available, to obtain the R_0 . Waber and Larson³⁸ recalculated ρ , χ and R_0 for a number of rare earth metals. These data are presented in Table III. Values are given for both divalent and trivalent forms of ytterbium and europium. The use of both valences is much more questionable in the case of lutetium.

Raimes⁵ pointed out that, aside from the systematic errors due to the approximations made in deriving the equations, one

ORIGINAL PAGE IS
OF POOR QUALITY

Table I. Comparison of the Calculated Values of the Metallic Radius ρ , Heat of Sublimation S and Compressibility χ with the Experimental Values. Values of the Total Electronic Energy E_T and Ground State Radius r_0 also used.

Element Considered	Radius r_0 , A.U.	Radius ^{ex} ρ A.U.	Heat S kcal/mole	Compress. ^{ex} $\chi \times 10^6$ cm ² /kg.	Total E_T kcal/mole
--------------------	---------------------	----------------------------------	--------------------	---	-----------------------

Trivalent Elements

Aluminum	2.132	3.190	26	0.78	1253
Exp.	-----	2.990	75	1.34	1302
Scandium	2.540	3.635	100	1.27	1117
Exp.	-----	3.427	80.8	-----	1097
Gallium	1.913	2.973	13	0.61	1332
Exp.	-----	3.161	66	2.0	1384
Yttrium	3.198	4.358	47.7	2.44	949.2
Exp.	-----	3.760	82.6	2.95	984.1
Indium	2.173	3.235	24	0.82	1238
Exp.	-----	3.478	59.1	2.5	1273
Lanthanum	3.466	4.653	60	3.22	894
Exp.	-----	3.921	99.5	3.24	922
Thallium	2.008	3.056	3	0.66	1301
Exp.	-----	3.577	43	2.77	1341

Tetravalent Elements

Silicon	1.846	2.875	-46	0.298	2354.8
Exp.	-----	3.184	105	1.00	2497.6

Table I. (continued)

Element	Radius	Radius	Heat S	Compress.	Total E_T
Considered	r_0 , A.U.	ρ A.U.	kCal/mole	$\chi \times 10^6$ cm ² /kg	kCal/mole
Titanium	1.948	2.988	95	0.342	2195
Exp.	-----	3.178	111.1	0.868	2212
Germanium	1.816	2.842	-21	0.290	2370
Exp.	-----	3.308	89	1.364	2480
Zirconium	2.615	3.735	82	0.810	1864
Exp.	-----	3.347	142.2	1.106	1942
Hafnium	2.672	3.799	29	0.816	1836
Exp.	-----	3.301	168	0.881	1975
Thorium	3.077	4.256	17	1.321	1657
Exp.	-----	3.754	127	1.846	(1760)

Pentavalent Elements *

Vanadium	1.634	2.628	169	0.14	3869
Exp.	-----	2.817	122	0.609	3892
Niobium	2.237	3.310	75	0.34	3163
Exp.	-----	3.071	185	0.57	3273

* The experimental values of the Wigner-Seitz radius were obtained from the volumes V cm³ per gram atom listed by Teatum, Gschneidner and Waber³², using the formula $\rho = 1.3880 \sqrt[3]{V}$.

**Experimental compressibilities are for 343°K.

Table II Unpublished Calculations by Raimes

METALS OF HIGHER VALENCY

Metal	Lattice Constant ρ (Å)		Compressibility $10^{12} \chi$ (cm ² /dyne)		Cohesive Energy S (Kcal./mole)		Deviation ΔS as % Fermi E
	<u>Calc.</u>	<u>Obs.</u>	<u>Calc.</u>	<u>Obs.</u>	<u>Calc.</u>	<u>Obs.</u>	
Trivalent Metals							
Al	1.72	1.58	0.9	1.4	8	55	-12
Sc	1.99	(1.8)	1.5	---	75	70	2
Y	2.36	1.97	2.8	---	28	90	-29
Ga	1.60	1.67	0.7	2.1	- 6	52	-12
In	1.74	1.84	0.9	2.7	6	52	-11
Tl	1.65	1.89	0.7	2.3	- 17	40	-13
Tetravalent Metals							
Ti	1.61	1.62	0.4	---	132	100	4
Zr	2.02	1.71	0.9	---	14	110	-20
Sn	1.74	1.86	0.5	1.9	- 36	78	-18
V	1.42	1.48	0.2	---	100	85	+ 1
Semi-Conductors							
Si	1.55	1.68	0.3	0.3	- 63	85	-18
Ge	1.53	1.74	0.3	1.4	- 59	85	-17

*The author is indebted to Prof. Raimes who made this information available for use.

Table III. Comparison of Results Obtained in Recent Cohesive Energy Calculations for the Lanthanide Metals

	Wigner-Seitz Radius ρ (Bohr Units)			Compressibility $-\chi \cdot 10^6 \text{ cm}^2/\text{kg}$			Parameter R_0 (Bohr Units)	
	BS	LW	OBS.	BS	LW	OBS.	LW	BS
Sc(3)	3.69	3.635	3.427	1.37	1.27	----	2.54	2.56
Y(3)	4.40	4.358	3.760	2.69	2.44	2.95	3.198	3.20
La(3)	4.70	4.653	3.921	3.47	3.22	4.13	3.466	3.47
Ce(3)	4.65	4.464	3.81(γ)	3.29	2.75'	4.10(γ)	3.295	3.42
Ce(4)	4.31	3.490	3.57(α)	1.58	0.61'	4.72(α)	2.387	3.09
Sm(3)	4.50	4.174	3.761	2.88	2.15	3.52	3.684	3.28
Eu(2)	4.84	4.829	4.290	8.13	7.76	4.91	3.715	3.67
Eu(3)	----	4.088	4.290	----	1.98	4.91	2.953	----
Yb(2)	4.54	4.485	4.044	6.33	5.92	7.84	3.389	3.28
Yb(3)	----	3.986	3.986	----	1.80	7.84	2.860	----
Lu(3)	4.25	3.771	3.628	2.36	2.51	2.33	3.198	3.06
Lu(2)	----	4.358	3.628	----	3.10	2.33	2.701	----

BS = reference 6

LW = reference 38

source of error in the cohesive energy arises from the estimation of the ground state energy; a two per cent change in $E_0(\rho)$ yields almost a 20 per cent change in S . It is shown in Fig. 1 that for certain regions of the ionization potential, an appreciable error could be made in determining R_0 by means of the Raimes equation due to the steps. Such errors would have a stronger effect on the ground state energy at $R_s = R_0$, than at $R_s = \rho$. However, here we will not go into problems of estimating R_0 accurately.

Brooks³⁹ presented a simplified theory of cohesion which involved a modification of the quantum defect method used by Kuhn⁴⁰ to determine $E_0(R_0)$. Values of r_0 determined in this way are compared in Table IV with those computed herein. The equilibrium radius ρ was evaluated using Equations (8) and (9) as above. The values of ρ obtained in these two ways are also compared with the experimental value in Table IV. It will be seen that Brooks' small r_0 values result in better agreement with the experimental radii. Also the experimental values of S for the five metals studied by Brooks agree with his calculated values better than they do with those calculated by the present method.

The Wigner-Seitz radius ρ and cohesive energy of the noble metals, copper, silver and gold are compared with experimental values in Table V. Brooks¹ noted that the experimental values of S for these monovalent metals were three or four times larger than the values of S/N for any of the other 32 elements he considered. He concluded that the closed d-shells contribute significantly to the binding. It is interesting that for the IIB, IIIB and IVB elements which follow these transition metals in the Periodic Table, the binding is normal and the values of S/N lie in the same range as mentioned in the first part of this paper. Thus the ion cores are more effectively separated from each other by the gas of free electrons; an error arises when

Table IV. Comparison of the Brooks' Values of R_0 and ρ with Present Computations of these Radii in Atomic Units

Element Treated	Ground State Radius R_0		Wigner-Seitz Radius, ρ		
	Brooks	Present	Present	Brooks	Exper.
Na	2.97	3.244	4.147	3.886	3.991
Mg	2.38	2.563	3.601	3.437	3.345
Al	2.03	2.132	3.190	3.088	2.990
Si	1.755	1.846	2.875	2.75	3.184
Zn	-	2.003	3.024	2.784	2.904

Table V. Comparison of Calculated and Experimental
Values for the Noble Metals (after Brooks¹)

	Cohesive Energy, δ		Wigner-Seitz		Compressibility	
	Rydbergs/electron		Radius, Bohr Units		$\chi \times 10^6 \text{ cm}^2/\text{kg}$	
	Calc.	Exp.	Calc.	Exp.	Calc.	Exp.
Copper	0.087	0.260	2.608	2.669	2.80	0.734
Silver	0.086	0.221	2.666	3.017	3.03	1.004
Gold	0.085	0.264	2.146	3.012	1.43	0.570

one assumes that the d-electrons are confined to a very small region associated with the ion core and have negligible probability of being found at the cell boundary. This is equivalent to the old tight binding approximation which is inadequate for transition metals.

Typical behavior of the calculated compressibility χ as a function of pressure is shown in Fig. 4 for four tetravalent metals.

In the noble metals, the interatomic distance, however, is governed by the interaction between d-electrons and the ion cores. Contrary to the trend found for most metals in Table I, the calculated values of ρ in Table V are less than the observed values. Thus, one would anticipate that, due to ionic repulsion, the actual compressibility of copper, silver and gold would be substantially lower than that calculated by the present method, which only includes electron-electron repulsions. This is borne out in Table V where the experimental χ values are only 0.3 to 0.4 that of the calculated values. Thus, it is reasonable to conclude that for these noble metals, the interaction between the valence electrons and those forming the ionic core is much stronger than in normal metals and that the present simple method is not satisfactory.

The importance of such repulsion is illustrated in the pressure-volume graph, Fig. 5, for nickel. As a shock wave passes through a metal, it is subjected to large negative pressures during the rarefaction wave--although that portion is not plotted in Fig. 5. As an atom, nickel has only one 4s electron to act as a valence electron. To incorporate the effect of the 3d electrons, we have assumed that N is higher than two. In doing the calculations, N=3 gives better agreement with the experimental shock wave data⁴¹.

A more significant way⁷ of dealing with the ion cores is to add

$$E_{\text{ionic}} = b \exp\left(\frac{-S_{ii}}{\rho_{\text{BM}}}\right) \quad (14)$$

to the terms in Equation 9.

Fig. 4.

The calculated pressure dependence of χ for four different tetravalent metals.

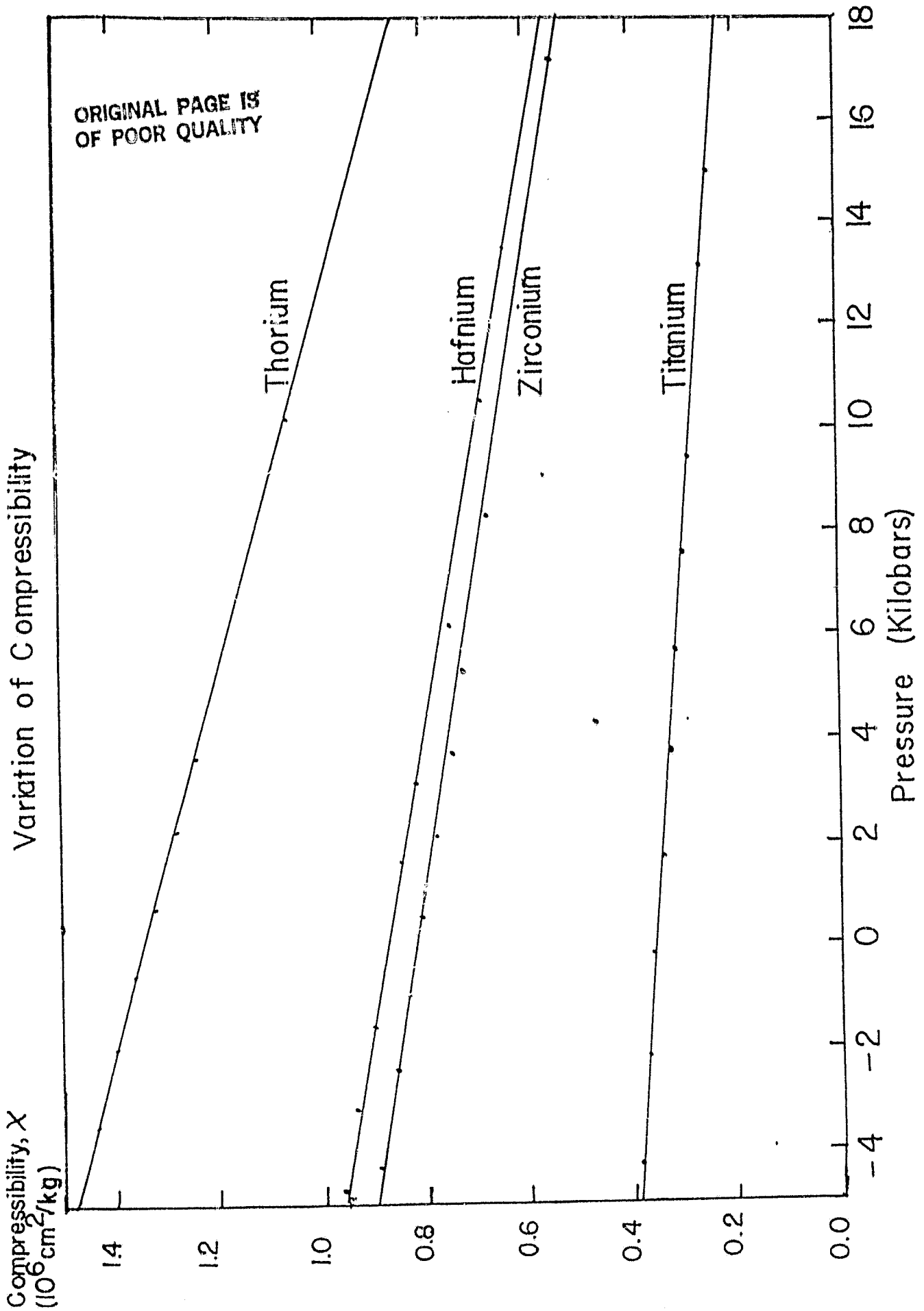
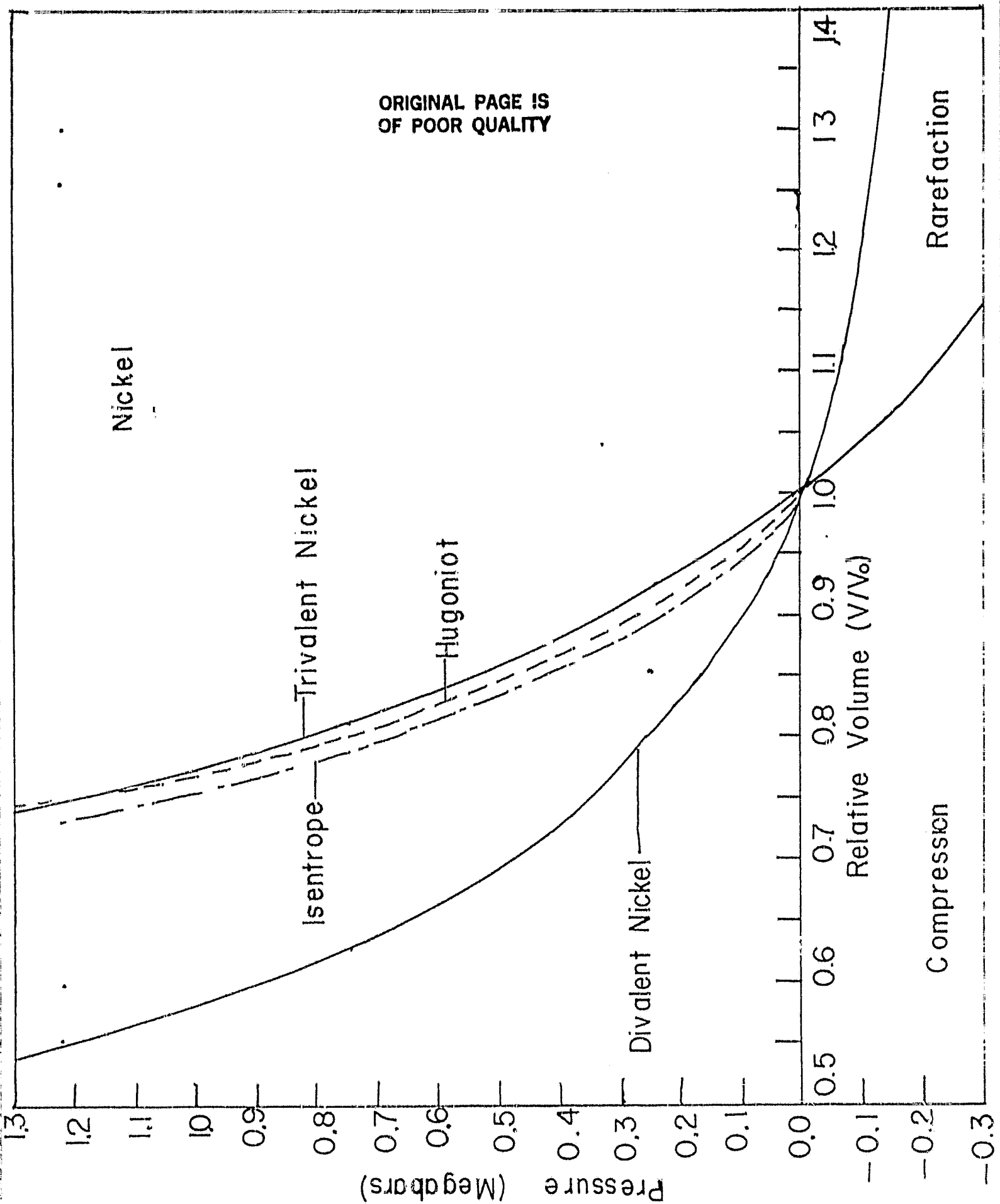


Fig. 5.

Comparison of experimental shock wave data of McQueen and Marsh for nickel with two calculated P versus V curves.



Here b is an adjustable constant approximately equal to 10^{12} ergs and S_{ij} is given by

$$S_{ij} = r_{ij} - r_i - r_j \quad (15)$$

where r_i and r_j are the ionic radii such as most chemists use. Concerning the repulsive parameter ρ_{BM} which occurs in the Born-Mayer expression for ionic crystals, Hafnestein and Zahrt⁴² showed that values of ρ_{BM} could be calculated directly from overlap integrals -- normally it is an experimentally adjustable quantity approximately equal to $0.345A^0$. We have established that including ionic terms improves the agreement with shock wave data on gold as Fig. 6 shows. Inasmuch as the inclusion of ionic repulsion has been made only for limited cases here, it would take us away from the main theme of this paper to go into further detail about how the quantities b and ρ_{BM} are estimated. This will be discussed in a forthcoming paper.

Application of the Fröhlich-Raimes Model to Alloys

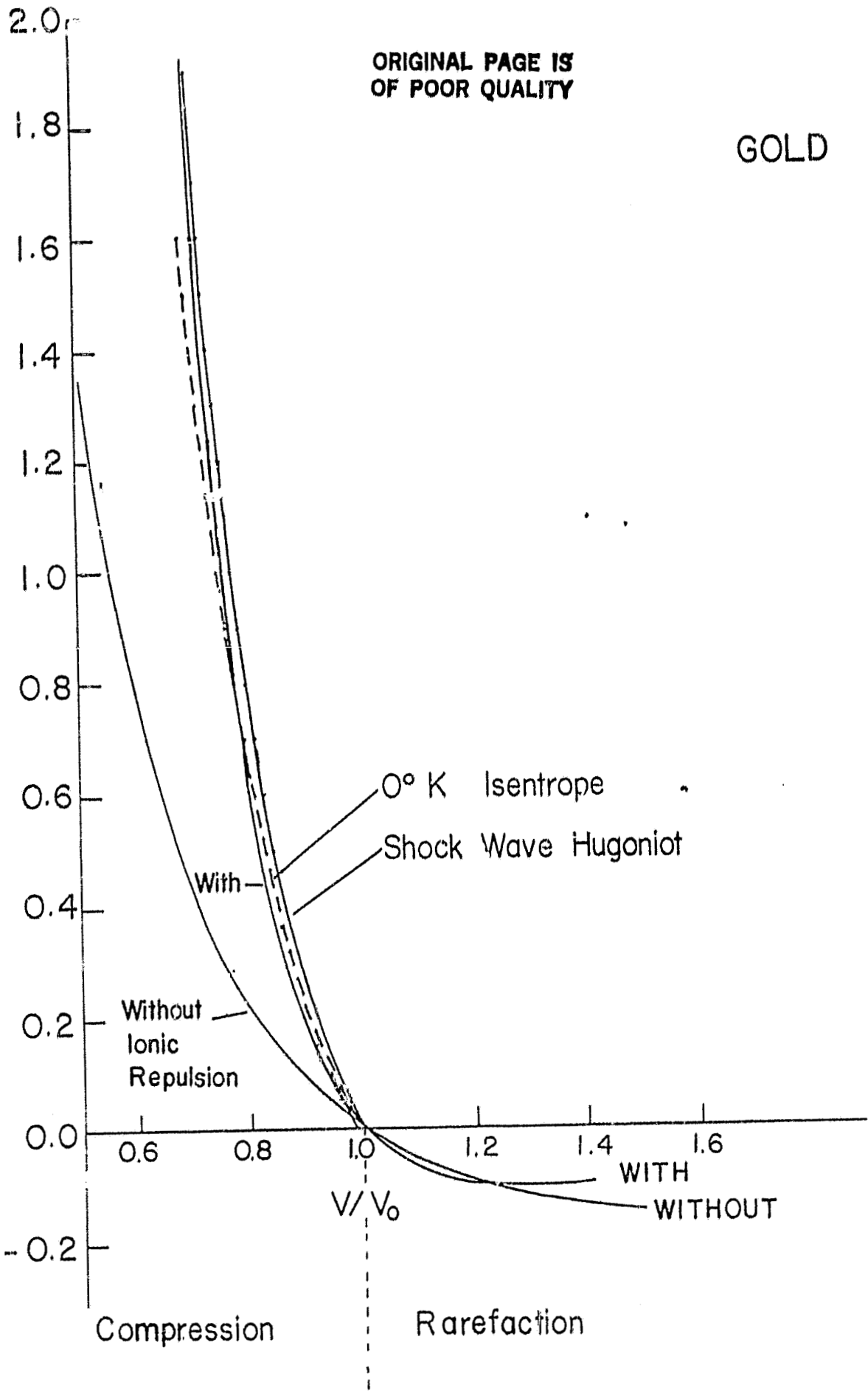
The Fröhlich-Raimes method has been applied to alloys³⁸. One reasonable assumption is that the ground state energy of the alloy is given by a linear combination of E_0 terms. That is,

$$-E_0(C_A, R_S) = \frac{C_A n_A}{R_S} \left(3 - \frac{R_S^2}{R_{0A}^2} \right) + \frac{C_B n_B}{R_S} \left(3 - \frac{R_S^2}{R_{0B}^2} \right) \quad (16)$$

where C_A , n_A and R_{0A} are, respectively, the atomic concentration, the valence and the Fröhlich-Raimes parameter for component A, and R_S is the variable radius of a Wigner-Seitz sphere. Here it is assumed that $\beta=0$. For the interaction energy, the mean number $C_A n_A + C_B n_B$ of valence electrons was used. This \bar{n} is inserted in the remaining terms of Equation 9 rather than averaging the two E_c values. To distinguish expressions, we will denote the total energy of an alloy by E_c . Values E_c , radius ρ , and compressibility χ have been obtained as a function of concentration for a large number of alloys. Most of these results

Shock wave data for gold.

Megabars



will be reported elsewhere, but one type of result will be summarized here.

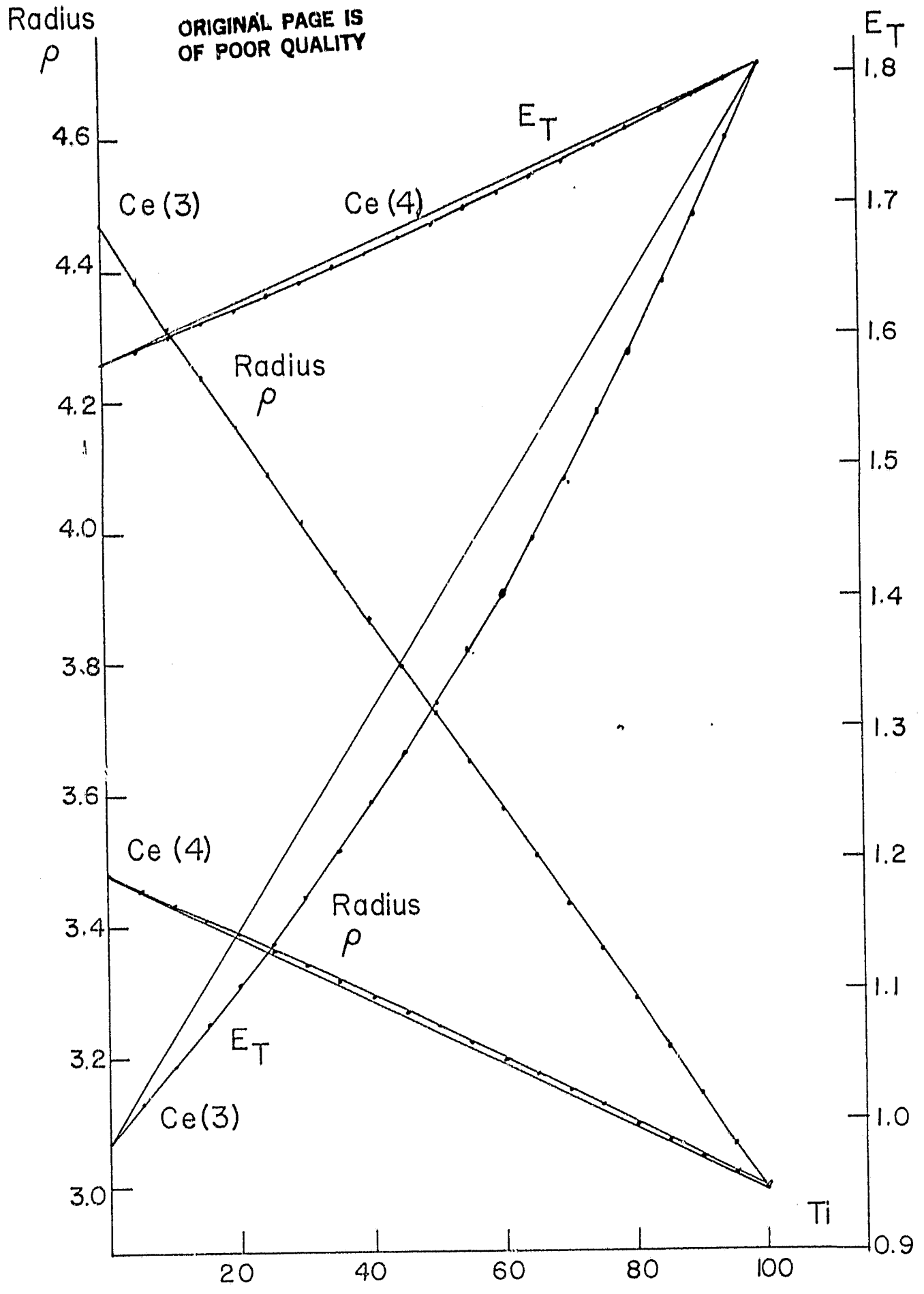
It has become common for metallurgists to compare the observed average lattice spacing of alloys with the spacing of alloys with the spacing obtained by averaging the lattice spacings of the components. One can calculate $\rho(C_A)$ and compare it with Vegard's Law which states that the volumes of components are additive. We have assessed this deviation from Vegard's Law by computing

$$-y(C_A) = \rho(C_A) - (C_A \rho_A + C_B \rho_B) \quad (17)$$

Such deviations, $\Delta\rho(C_A)$ are illustrated in Fig. 7 for Ti and two different valences of cerium. A large negative deviation can be seen for the tetravalent Ce.

The total energy $E_t(C_A, \rho)$ has been plotted for three other binary systems. Fig. 8 is for Na-Ag for which little solubility exists at either end. However, the calculated curve cannot illustrate this feature. The large positive deviation from Vegard's Law which can be seen in the plot of $\rho(C_A)$ is the clue. Of course, strain energy in the lattice has not been included in the present model. So direct evidence for phase separation cannot come from the intentionally restricted model used at the present time. Fig. 9 is for Na-Mg alloys. The heat of formation of these alloys ΔE is the deviation from the straight line which would be given by a mechanical mixture. In almost all cases studied, the solid solutions would tend to be more stable than a two phase mixture. Note that this stability does not result from including the usual entropy of mixing but is strictly electronic in origin. No electronic entropy term has even been included. Both would increase the stability of any solid solution.

The results of a large number of calculations about Vegard's Law are summarized in Table VI. In some cases, there is experimental evidence for positive and negative deviations. In a number of cases predictions are made which may be verified using additional lattice parameter data not readily available to the author when this summary was originally made.



Na - Ag

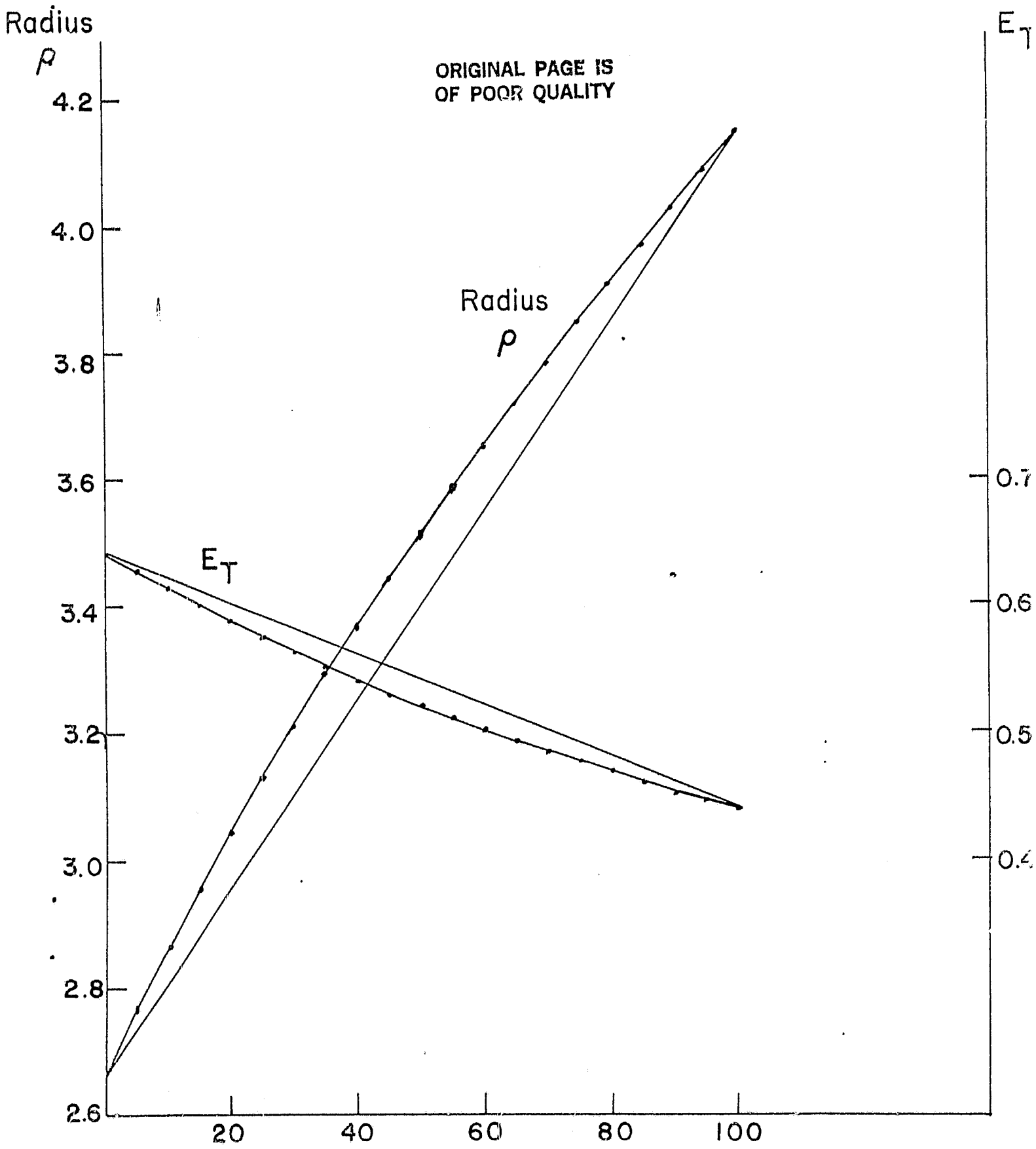


Fig. 9.

Na - Mg

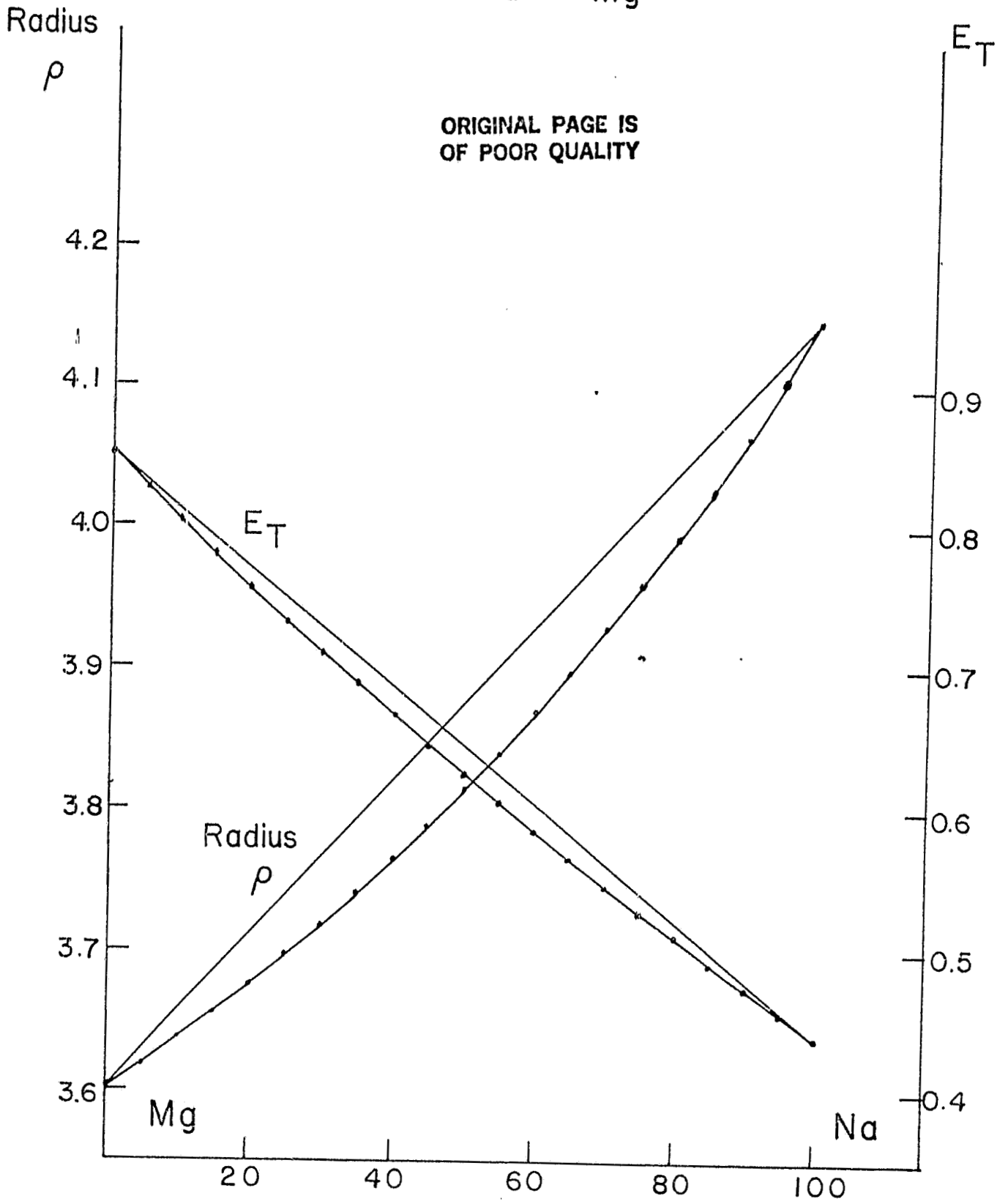


Table VI.

Comparison of Calculated Deviation from Vegard's Law with Observed Deviation

Binary System	C _A at Max. Calc. Δρ ³	Calc. 100 Δ[ρ(C _A)]	Experimental Deviation			Calc. 100 Δ[ρ ³ (C _A)]	Deviation of	
			Cubic a ₀	Hexagonal a ₀	c ₀		Cell Vol.	Non-Cubic
Monovalent Solvent								
K-Rb	0.5	+0.15	neg.	----	----	-0.07		
K-Cs	0.5	+1.08	neg.	----	----	-0.58		
Cs-Rb	0.5	+0.43	neg.	----	----	-0.24		
Na Mg	0.55 Na	----	----	----	----	-3.58		
Na Ag	0.45 Na	----	----	----	----	-1.73		
Na Zn	0.55 Na	----	----	----	----	-6.98		
Divalent Solvent								
Mg-Li	0.45 Mg	-3.38	neg.	neg.	neg.	-1.63		
Mg Zn	0.5	+1.65	----	none	none	-0.28		
Mg Sn (2)	0.5	-0.04	----	pos.	neg.	-0.01		
Mg Al	0.55 Mg	-27.00	----	neg.	neg.	-1.38		
Mg Ga	0.55 Mg	-3.49	----	neg.	neg.	-2.11		
Mg In	0.55 Mg	-2.53	----	pos.	pos.	-1.23		
Mg Tl	0.55 Mg	-3.27	----	pos.	neg.	-1.83		
Mg La	0.5	+12.80	----	pos.	pos.	+3.32		
Mg Ce (3)	0.55 Mg	+10.20	----	only one point		+2.77		
Mg Ce (4)	0.55 Mg	-1.75	----	only one point		-0.70		
Mg Sn (4)	0.55 Mg	-5.75	----	pos.	neg.	-2.46		
Mg Bi	0.55	-3.39	----	neg.	neg.	-1.97		
Ca Sr	0.50	+0.40	neg.	----	----	-0.17		
Ca Ba	0.50	+2.50	neg.	----	----	-1.23		
Ba Sr	0.50	+0.91	neg.	----	----	-0.48		
Ca Zn	0.50	+9.85	----	----	----	-2.40		
Ca Ti	0.55 Ca	-13.09	----	----	----	-12.67		
Ca Mn	0.55 Ca	-21.26	----	----	----	-20.76		
Ca Cr.	0.55 Ca	-30.51	----	----	----	-23.39		

Note: The linear combination of volumes $C_A \rho^3(C_A) + C_B \rho^3(C_B)$ does not lead to the same deviations (occasionally even differing in sign) as does the linear combination of cell diameters as used in Eq.

ORIGINAL PAGE IS
OF POOR QUALITY

Table VI. (cont.)

Comparison of Calculated Deviation from Vegard's Law with Observed Deviation

Binary System	C_A at Max. Calc. $\Delta\rho^3$	Calc. $100 \Delta[\rho(C_A)]$	Experimental Deviation			Calc. $100 \Delta[\rho^3(C_A)]$	Deviation of	
			Cubic a_0	Hexagonal a_0	c_0		Cell Vol.	Non-Cubic
<u>Trivalent Solvent</u>								
Al Ca	0.45 Al	-4.09	neg.	----	----	-7.38		
Al Zn	0.45 Al	+1.59	pos.	----	----	+0.40		
Al-La	0.50	+8.36	insufficient data			-2.35		
Al-Ce (3)	0.50	+6.55	pos.	----	----	-1.73		
Al-Ce (4)	0.50	+2.25	pos.	----	----	+0.54		
Al-Ti	0.55 Al	-1.09	none	neg.	pos.	-0.41		
Al Mn	0.55 Al	-5.64	----	----	----	-2.92		
Al Cr	0.55 Al	+9.19	----	----	----	-3.52		
<u>Tetragonal</u>								
				a_0	c_0			
In-Cd	0.45 In	-1.05	----	pos.	----	-0.39		
In-Sn (2)	0.45 In	-3.01	----	pos.	pos.	-1.65		
In-Pb (2)	0.45 In	+2.54	----	pos.	pos.	-1.24		
In-Tl	0.50	+0.17	----	pos.	pos.	-0.03		
In-Sn (4)	0.50	-0.49	----	pos.	pos.	-0.16		
In-Pb (4)	0.50	-1.02	----	pos.	pos.	-0.38		
In-Sb	0.55 In	-2.52	----	----	----	-0.87		
<u>Tetravalent Solvent</u>								
Ti Ca	0.45 Ti	-13.09	----	neg.	neg.	-12.67		
Ti Zn	0.42 Ti	-0.53	insufficient data			-0.15		
Ti-Sn (2)	0.40 Ti	----	----	neg.	pos.	-4.04		
Ti Al	0.45 Ti	-1.09	----	neg.	pos.	-0.41		
Ti-Ce (3)	0.45 Ti	----	insufficient data			-6.22		
Ti La	0.45 Ti	----	----	----	----	-7.66		
Ti Zr	0.50	+2.60	none	none	none	-0.52		

ORIGINAL PAGE IS
OF POOR QUALITY

Table VI. (cont.)

Comparison of Calculated Deviation from Vegard's Law with Observed Deviation

Binary System	C. at Max. Calc. $\Delta\rho^3$	Calc. $100 \Delta[\rho(C_A)]$	Experimental Deviation			Calc. $100 \Delta[\rho^3(C_A)]$	Deviation of	
			Cubic a_0	Hexagonal a_0	c_0		Cell Vol.	Non-Cubic
Tetravalent Solvent (cont.)								
Ti Ce (4)	0.50	----	insufficient data			-0.21		
Ti Sn (4)	0.50	----	----	neg.	pos.	-0.22		
Ti Hf	0.50	+3.03	neg.	neg.	pos.	-0.62		
Ti Th	0.50	----	none	----	----	-1.64		
Ti V	0.50	----	pos.	----	----	-0.54		
Ti Mn	0.55 Ti	-0.63	----	----	----	-1.06		
Ti Nb	0.50	+2.16	neg.	neg.	neg.	-0.40		
Ti Cr	0.55 Ti	+3.57	neg.	none	none	-1.57		
Ti Mo	0.55 Ti	----	neg.	neg.	neg.	+0.10		
Zr Hf	0.50	+0.02	pos.	none	none	-0.004		
Zr Nb	0.50	+1.36	neg.	neg.	neg.	-0.98		
Hf Nb	0.50	-1.44	pos.	----	----	-1.18		
Zr La	0.45 Zr	----	----	----	----	-4.09		
Zr Ce (3)	0.45 Zr	----	----	----	----	-0.21		
Zr Ce (4)	0.50	----	----	----	----	-2.95		
Zr Th	0.50	----	----	----	----			

The calculated data in Table VI are arranged by the valence of the solvent. The cases treated were for binary systems cited by Pearson⁴³ in his large tabulation of lattice parameters. Without becoming involved in detailed evaluation of the experimental deviations of different alloys, as well as making a decision about the comparative reliability of specific experimental data, it appeared to be sufficient at this time to report the sign of the deviation. One complication, for example for magnesium based alloys, is that small alloy additions do not stabilize the α cubic phase. Since the C/a ratio of Mg is not ideal, packing of individual spherical cells in which the electrons exert a pressure can not be the sole criterion for determining the volume. Some modification of the model to include either structure sensitive properties or perhaps covalent bonding may be necessary to understanding the lattice dimensions in these alloys.

One illuminating test of this simple electron gas theory is the group IVb metals such as titanium, zirconium and hafnium, which do exist in both cubic and hexagonal modifications. In the upper portion of this drawing, the a_0 is plotted for the cubic phase Zr-Ti alloys. However, in the middle portion, two separate branches are shown for the a_0 parameter of hexagonal Zr based and Ti based alloys. The associated c_c values are presented in the lower portion of Fig. 10. These might be interpreted in terms of the definitely positive deviation from Vegard's Law presented in Fig. 11. Phase separation to the larger cubic phase would be compatible with the present model. At this time it is not clear why hafnium-niobium alloys remain cubic nor why the Zr-Hf do not form a cubic β phase.

The relative deviations $100y(C_A)/\rho_A$ can be used to reduce confusion about units, and values are presented in Table VII for cerium based alloys containing 10 per cent of several solutes. The relative deviations have the correct sign in both thorium-poor solid solutions when compared with the recent data of Waber, Harris and Raynor⁴⁴ but are smaller in magnitude than the observed values (4.14 for α and -1.31 for γ). The relative deviations they computed using Friedel's Elastic Model^{45,46} are similar (3.14 for α and -0.57 for γ) to those listed above.

INSERT PAGE 16a HERE, FOLLOWING END OF PAGE 16
16

Variation of Lattice Parameters of Solid Solutions

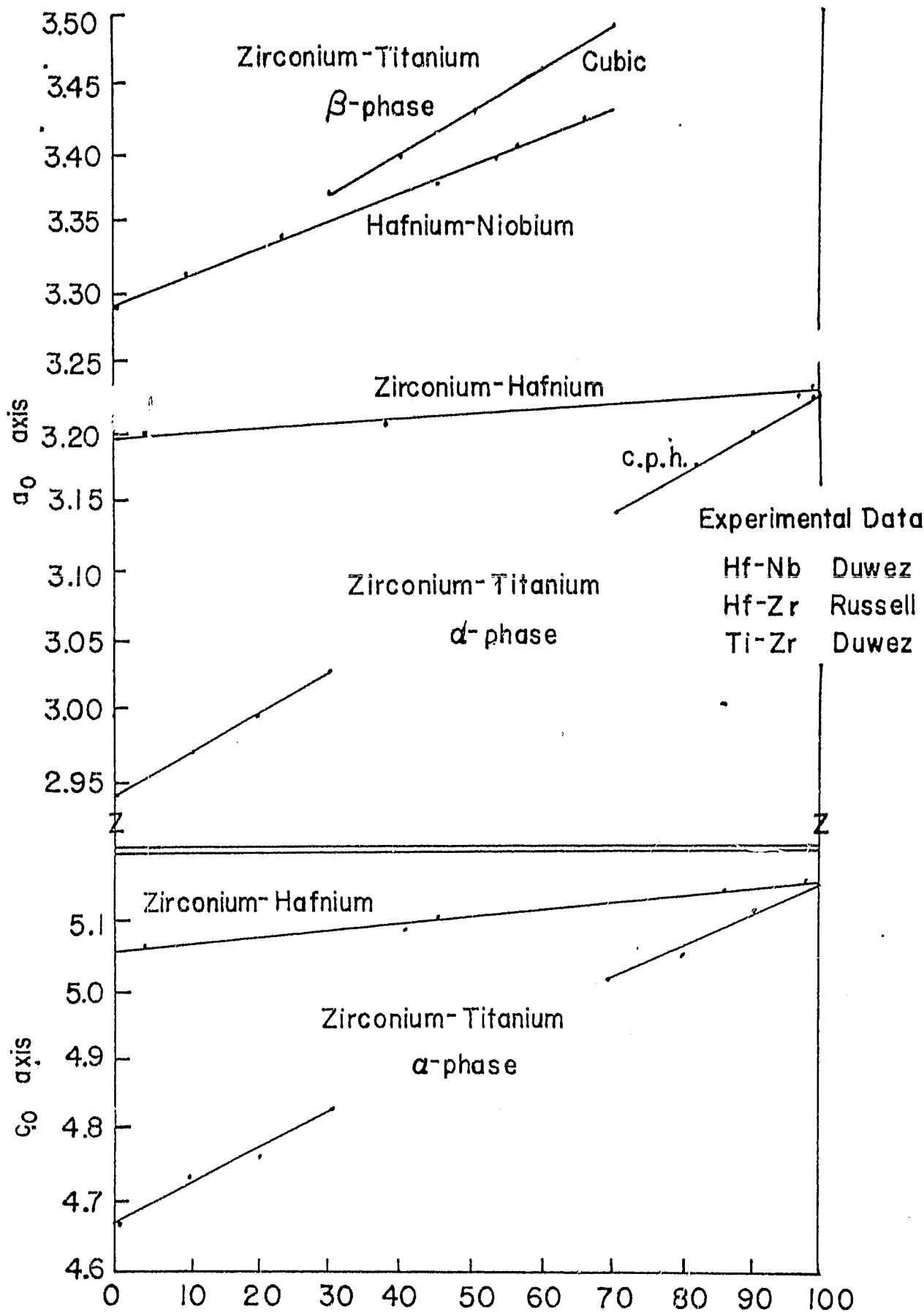


Fig. 11.

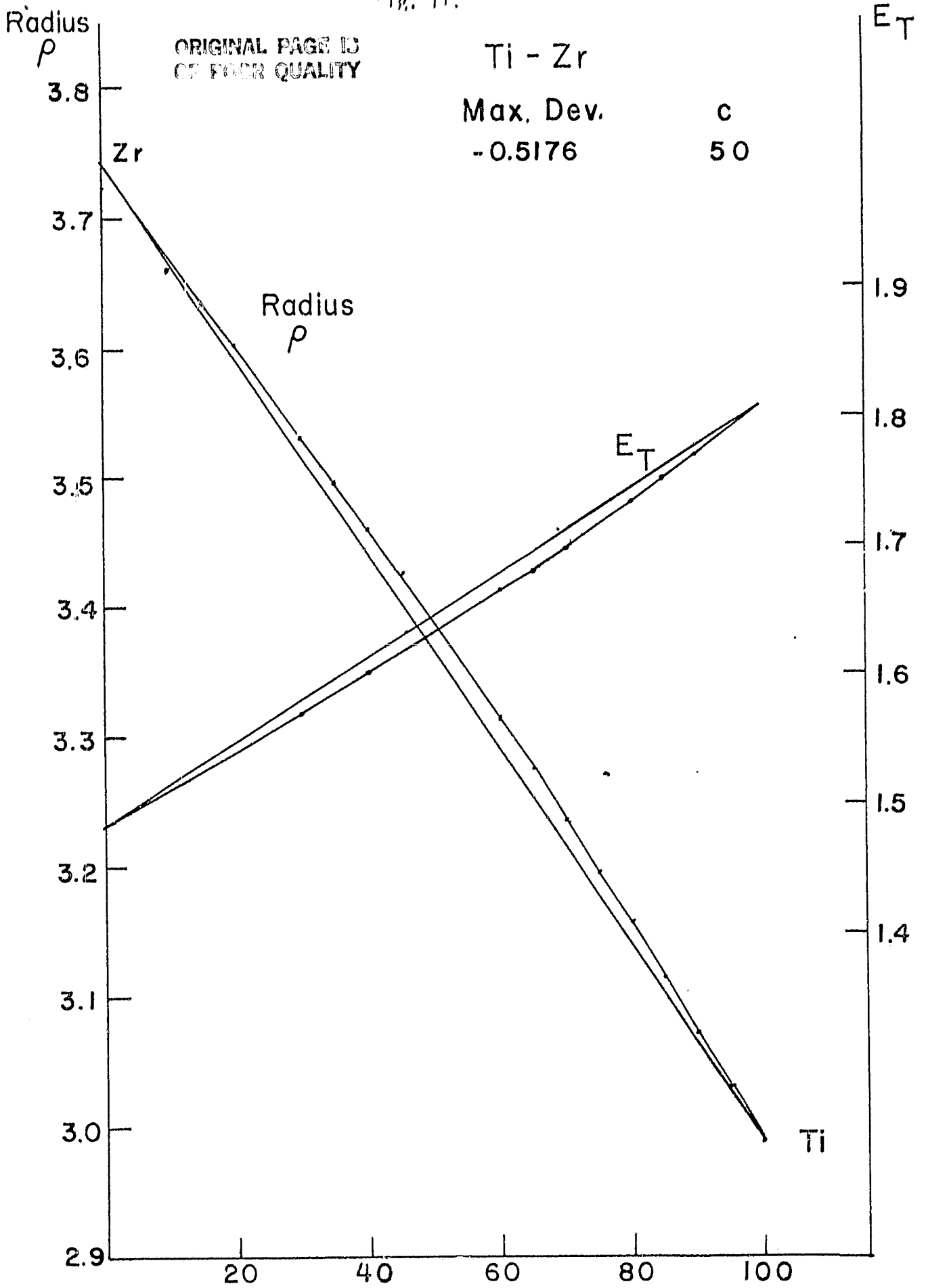


Table VII. Relative Deviations from Vegard's Law
 Calculated for Cerium-Base Alloys

Solute	Alpha Ce	Gamma Ce
Magnesium	-1.47	+6.75
Aluminum	2.07	+4.57
Lanthanum	-1.84	-0.09
Zirconium	+0.32	-2.29
Thorium	+2.73	-0.89

The sign of $\gamma(C_A)$ does agree with that reported by Gschneidner for dilute Mg alloys but does not agree well with the findings of Harris and Raynor⁴⁷ for cerium dissolved in α -Zr.

Davison and Smith⁴⁸ estimated the enthalpy of formation of CaMg_2 in a relatively similar manner. They indirectly allowed for the shift in the bottom of the band $E_0(R_S)$ with concentration. The volume of the intermetallic compound was found from the equation

$$\frac{4\pi}{3} R^3 = \frac{4\pi}{3} \left(C_A R_{SA}^3 + C_B R_{SB}^3 \right) \quad (18)$$

Further, they assumed that R_{SA}/R_{SB} was 1.225 to correspond to a Laves phase. In this author's opinion, it would have been preferable to have estimated the average number of electrons per atom and the calculated ρ and E_c values. They used Brooks' values of R_0 for Ca and Mg. Their data are presented in Table VIII. Smith⁴⁹ has found this prescription works reasonably for a number of intermetallic compounds.

ORIGINAL PAGE IS
OF POOR QUALITY

Table VIII. Comparison of Three Physical Quantities for Laves
Phases Calculated by the Fröhlich-Raimes Method
with Experimental Values
(After Davison and Smith⁴⁸)

	Heat of Formation			Volume of Formation		Compressibility	
	$-\Delta H_f$ in kcal			$-\Delta V$ in \AA^3		χ in cm^2/kg	
	Smith	Brooks	Exp.	Calc.	Exp.	Calc.	Exp.
Ca Mg_2	9.8	11.2	3.2	5.66	5.66	265	3.77
Sr Mg_2	7.9	9.39	1.7	9.64	8.42	---	----
Ba Mg_2	2.8	5.69	0.5	15.35	7.03	---	----

One interpretation of the failure of Hf-Zr to separate into a cubic phase can be made in terms of the compressibility of the host lattices. As Fig. 4 shows, the χ values for Hf and Zr are very similar. In contrast, Ti is significantly less compressible. The present adaptation of the Fröhlich-Raimes model to binary alloys permits one to calculate the variation of χ with composition. A set of curves for Ti-Zr alloys is shown in Fig. 12. This results from evaluation of Eq. and not from a simple scaling of the two P-V curves for the pure metals. We have not verified that the experimental compressibility of alloys is as variable as indicated by Fig. 12. The literature indicates that very little data has been collected. It seems that this would be a useful test which could be made of this volume dependent theory.

To summarize, the major features of this FR model for a metal and its alloys depend on the relation between the pressure and the density of electrons. This in turn depends on the volume in which they are confined. However, any details of the spatial arrangement of the atoms are ignored. As such, it leads to a good interatomic force law. In the Fröhlich-Raimes model it is assumed that the lowest energy of an electron $E_T(C_A)$ lies between E_T for one element and E_T for the other. Because of the simplicity of the FR model any Brillouin zone effects have not been dealt with.

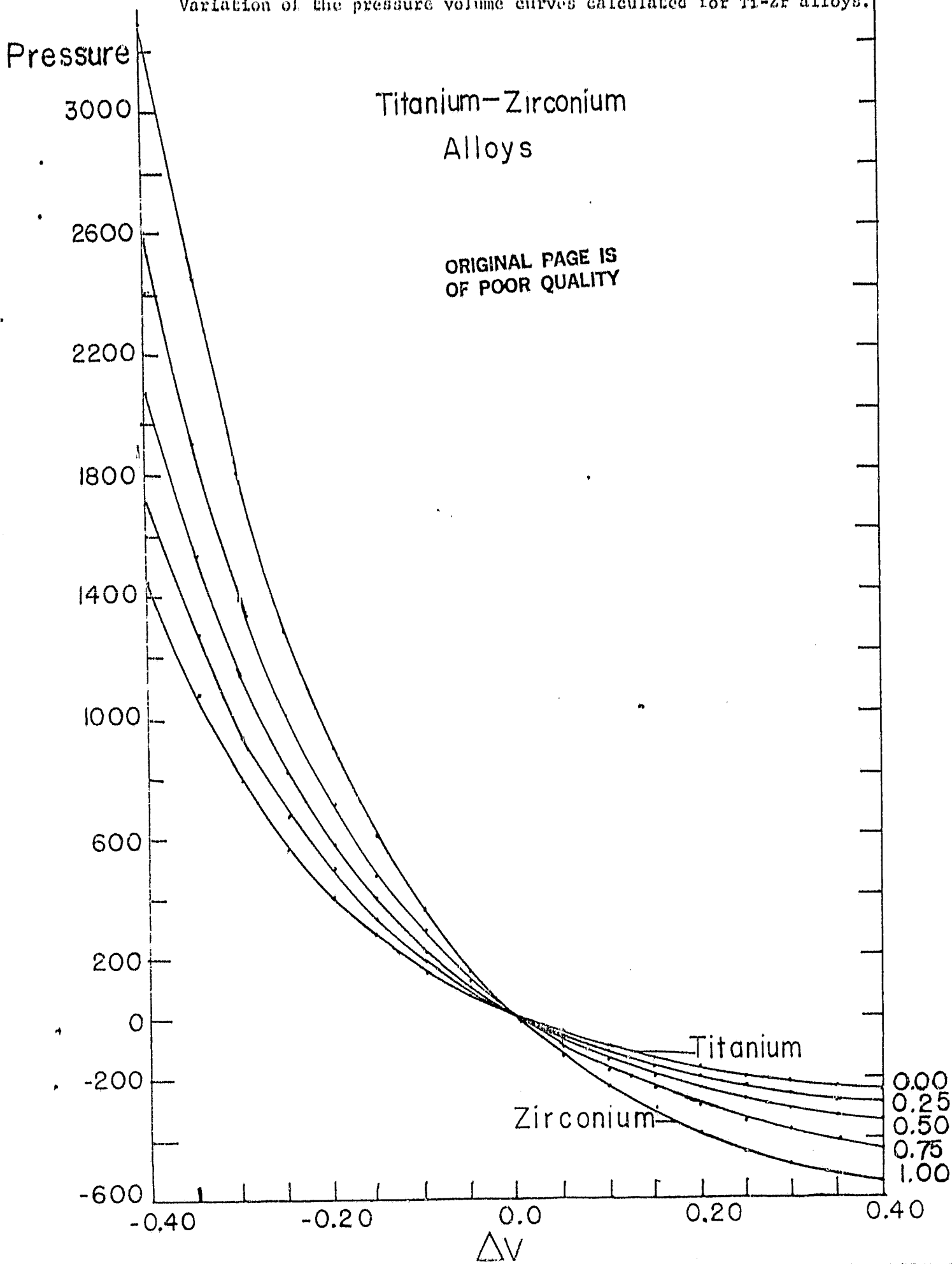
Electron Cell Model

In preparing this manuscript, the author came upon a very similar recent treatment of alloys by Bolsaitis and coworkers^{50,51,52}. It, too, is based on Fröhlich's equations¹. However, the spirit of their study is different since they have parameterized all terms and included several further thermodynamic corrections. They represent the cohesive energy by the equation

$$S = I_1 + \frac{A}{R_s^3} + \frac{F}{R_s^2} + \frac{B}{R_s} + E_{\text{corr}} + 6E_p + E_{\text{vib}} \quad (19)$$

FIG. 12.

Variation of the pressure volume curves calculated for Ti-Zr alloys.



Coefficient A could have been obtained from Eq. 3 and coefficient F could have been obtained by combining the remaining terms in Eq. 3 with the third term in Eq. 9. Since they dealt only with copper, silver and gold, B would have been equal to (1.2 - 0.916). Their E_p is given by Eq. 14 except that the r_i and r_j were not included in the numerator. They also included a Van de Waals attractive term C/R_s^6 , and a vibrational energy term. By virtue of having a considerable number of parameters to adjust, excellent agreement with the experimental data can be obtained. They introduced further arbitrariness when dealing with alloys by integrating the Grüneisen equation to get an entropy correction

$$S' = \int_{T_0}^T \frac{C_p - C_r}{T} dT = \int_{T_0}^T \alpha^2 V B_T dT \quad (20)$$

They further limited the ionic repulsive term from Eq. 14 to unlike pairs of atoms.

They varied the local charge density and cell radii according to Sanderson's¹³ stability ratios SR and in later papers, they used a definition given by Coulson for the stability. Both definitions assumed that the charge densities were uniform within an Electron Cell and could be scaled. Specifically, they chose the radius of the copper and gold atoms according to the prescription

$$\frac{\rho_{cu}(r)}{\rho_{au}(r)} = \frac{r_{au}^3}{r_{cu}^3} = \frac{SR_{cu}}{SR_{au}} \quad (21)$$

and the mean alloy volume

$$V = \frac{4\pi}{3} (x_{cu} r_{cu}^3 + x_{au} r_{au}^3) \quad (22)$$

Since neither radius is its equilibrium value, they estimate the volume of Mixing V_M by replacing r_{au} and r_{cu} by their equilibrium values r_{au}^0 and r_{cu}^0 in the parenthesis and then multiply it by $(1+V_M)$. This is an ad-hoc but plausible procedure.

Let us turn now to a second simple model which depends on knowing the band structure of each component. This model is sensitive to the details of the crystal arrangement. In general, it is available for only one interatomic distance and a complicated calculation is needed for each atomic volume as subtle changes may occur in the relation of one band or $E(k)$ curve to another. For practical reasons, the following model may be regarded as independent of the atomic volume.

LINEAR COMBINATION OF DENSITY OF STATES

In the basic theory of band structures, one allows one state and two spins for each atom in the piece of metal, and in general, the discrete spectrum of $E(k)$ is replaced by a continuum if 10^{23} atoms are involved. One observes that when one discusses impurity effects in semiconductors, the interesting case occurs when the impurity level lies in the gap between the conduction and the valence bands. Since the individual impurities are far apart in general, and are screened by a dielectric medium between them, the levels can be treated as discrete. However, if several types of defects are present, several very narrow energy ranges and hence spikes appear in overall density of states. The height of these reflect to a reasonable extent how many impurity atoms of a given type are present. As a second observation, where band structure calculations for intermetallic compounds have been made, one can frequently assign energy ranges where the states in the $E(k)$ curves can be identified as coming primarily from states derived from one constituent. Examples of this are the important studies on β -CuZn alloys and isomorphic phases by Keith Johnson and his colleagues^{54,55}. The third observation comes from Soven's study of the Coherent Potential Model⁵⁶, for an AB alloy. This work shows a modest increase in $N(E)$ values near ends of the allowed range of energies for constituent A and constituent B where $N_A(E)$ and $N_B(E)$ do not overlap--otherwise the $N(E)$ curves appear additive.

These observations lead Koskimaki and Waber¹⁸ to propose as a working hypothesis that a simple linear combination of the two density of states would suffice to substantially model the case of randomly distributed solid solutions.

In order to do this adequately it is necessary to abandon the

traditional idea of measuring all states from the bottom of the energy range (usually a point in k -space called Γ). Both must be referred to a common energy. When the energies are measured with respect to vacuum the E_F values for different metals, they occur in a relatively small range. This important observation has been discussed by Snow and Waber¹⁴ whereas the bottom of each band falls (relatively) smoothly with the atomic number. The curves for the two pure metals are shown in Fig. 13.

The LCDS model gives answers readily if the $N(E)$ data is available for both constituents, and these alloy $N(E)$ curves are in good agreement with the experimental facts. In Fig. 14, a typical calculation of the composition dependent $N(E)$ curves are presented for a solid solution of copper and nickel. It is very interesting that the set of these curves obtained with the LCDS model show many of the features exhibited in alloy results of Eastman⁵⁷, and Spicer⁵⁸, who used photoemission spectroscopy and Clift, Curry and Thompson⁵⁹ who used soft X-ray spectroscopy. At least the morphology of the alloy $N(E)$ is compatible with experience. No detailed comparison is appropriate at this stage of development.

One observation might be made in passing. Since the individual values of E_F are similar in energy, no large transfer of electrons to one type of atom occurs. Charging effects such as those discussed at the recent conference⁶⁰ will be less than if one combined the $N(E)$ curves after the bottoms of the two bands had been aligned at the arbitrary zero.

Now to locate the Fermi level for the alloy, one knows that the number of electrons is $C_A n_A + C_B n_B$ if there are no major charge transfer effects. The bottom of the alloy band will occur at the lower energy of the two $N(E)$ curves although it may not be heavily weighted. One finds the mean number of valence electrons \bar{n} per atom from $C_A n_A + C_B n_B$. Then one fills up the weighted states of the linearly combined $N_A(E)$ and $N_B(E)$ data to contain \bar{n} electrons. Thus, the E_F^a values will have a definite composition dependence, as will $N(E_F^a)$. The curve obtained in this manner for copper-nickel alloys is presented in Fig. 14.

FIG. 13.
N(E) curves for pure copper and nickel.

ORIGINAL PAGE IS
OF POOR QUALITY

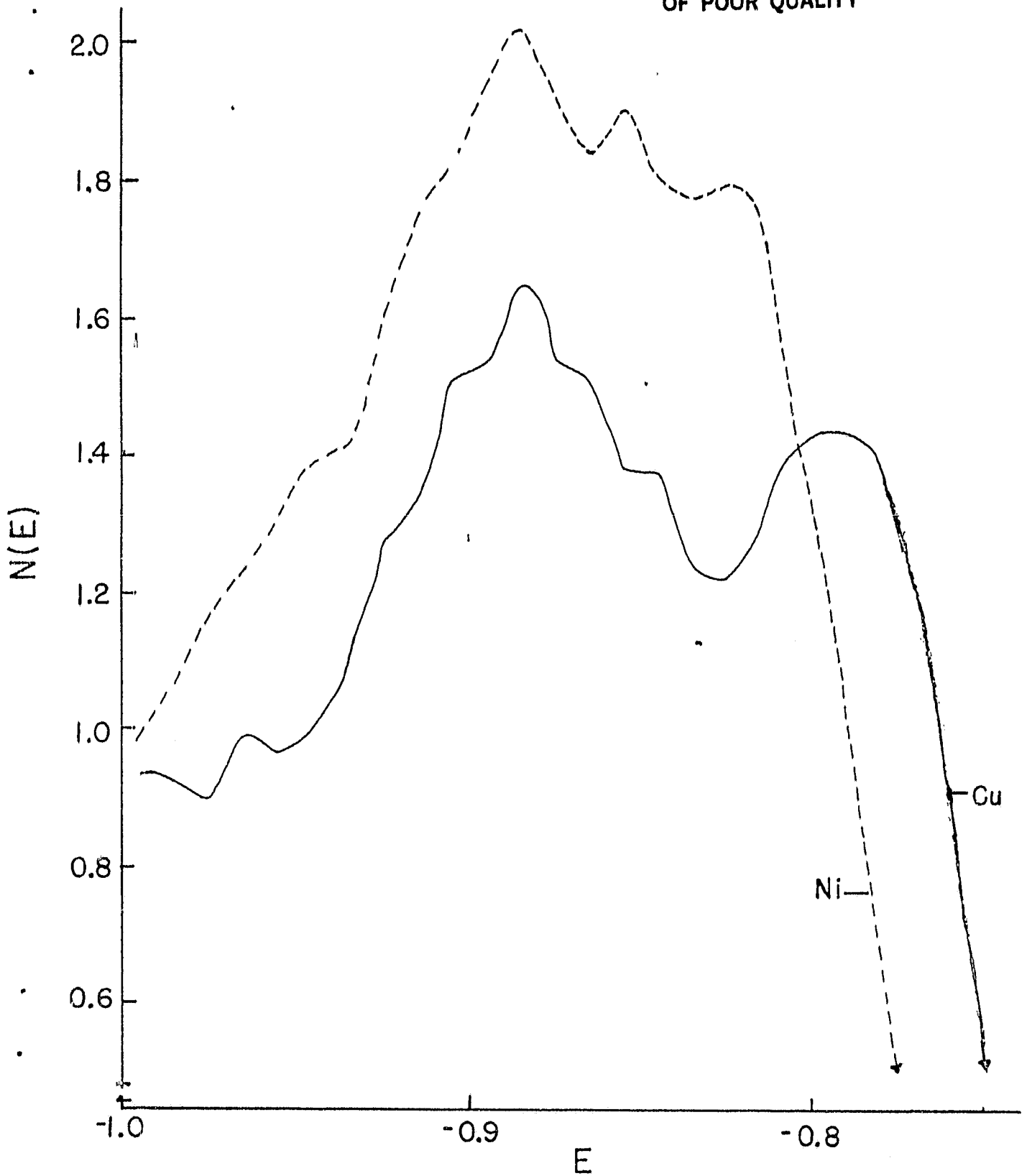
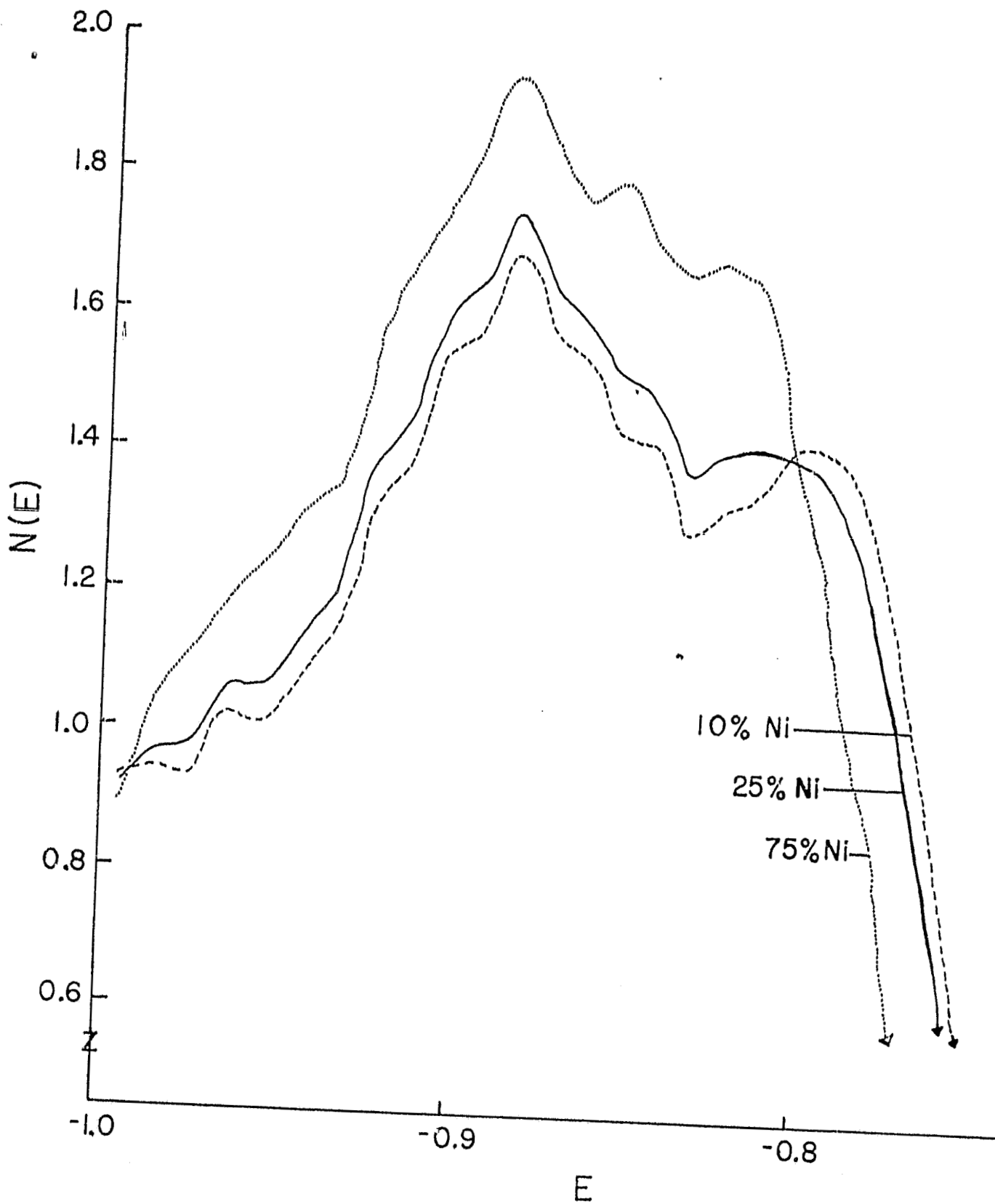


FIG. 14.

ORIGINAL PAGE IS
OF POOR QUALITY



For background information, the LCDS curves of $N(E_F^a)$ are presented in Fig. 15 for Ni and Al, and in Fig. 16 for Cu-Ni alloys. The decrease in $N(E_F^a)$ near 60 per cent solute has been attributed to filling of the d-states in nickel. Analysis of the data shows that some d-like states are unoccupied even when the concentration of solute exceeds the traditional amount needed at room temperature to fill 0.6 hole in nickel.

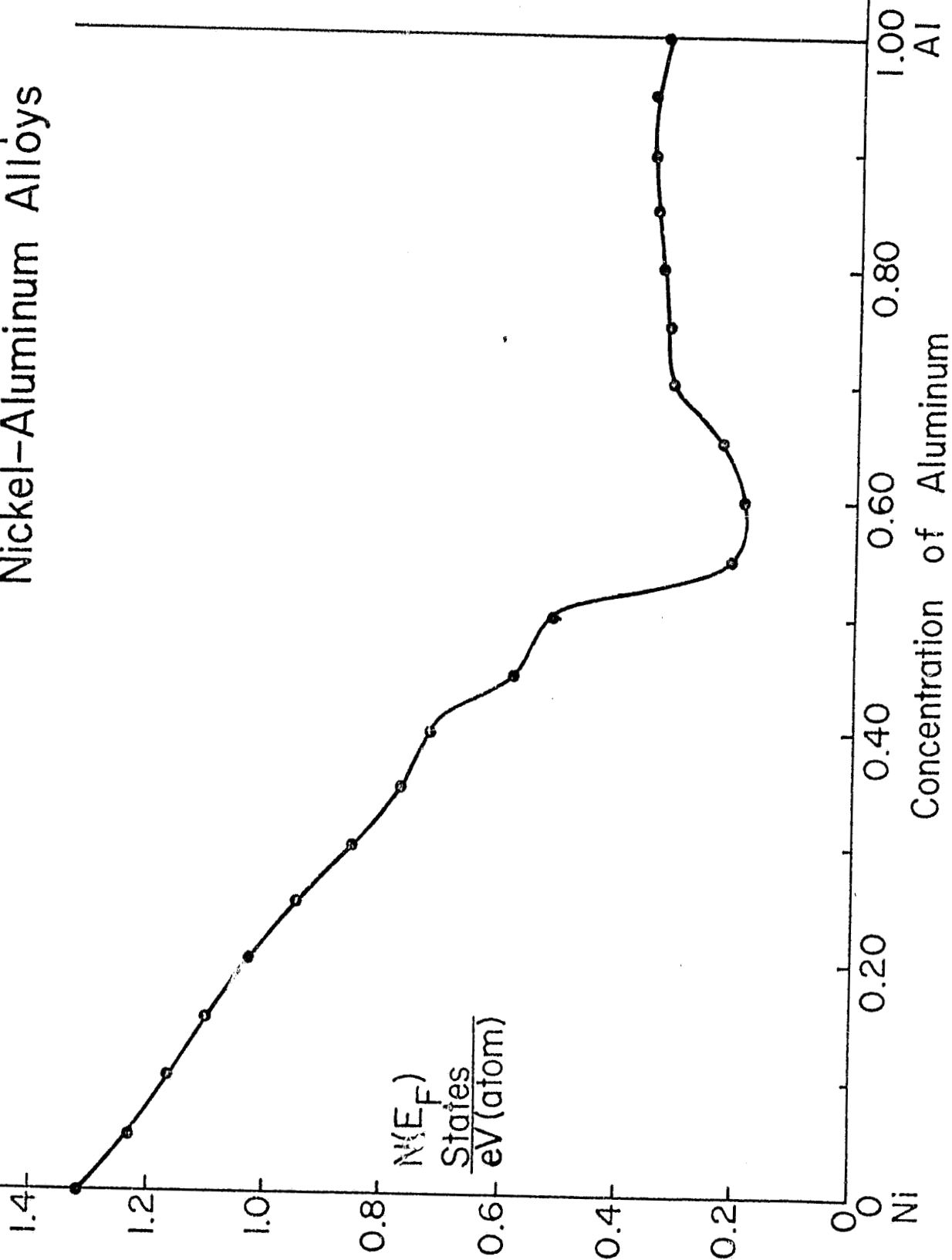
Examples of these $N(E_F^a)$ curves are presented for several binary alloys below. The curve for Ti plus Al in Fig. 17, is rather uninteresting since no sharp peaks and deep valleys occur in either of the component $N(E)$ curves.

The case of Ti plus V, which is shown in Fig. 18 is more interesting, particularly at the vanadium rich end. Two curves have been shown in Fig. 19 for the solution of Ti with Molybdenum. They are based on two different configurations of titanium, used as input to the APW program. It is more likely that the effective configuration in the solid BCC phase is d^3s^1 as Snow and Waber¹⁴ discuss. Despite whichever curve one chooses to use, the shape of $N(E_F^a)$ curve is surprising since one might at first, have anticipated simple curves with slowly changing slopes, as one saw for aluminum additions. The reason for the rapid variation of $N(E_F^a)$ with composition is because the individual $N(E)$ curves have a considerable amount of structure. One even more striking curve is that presented of $N(E_F^a)$ for zirconium and molybdenum in Fig. 20.

Before closing this topic, another illustration of the power of the LCDS model might be made. Calculations were done for the BCC and FCC forms of several pure metals. In the case of iron, calculations by Koskimaki and Waber⁶¹ showed that the α or BCC form of iron is more stable at room temperature than austenite. This was established by integrating $E \cdot N(E)$ over the occupied states. The transition energy occurs with the right sign, but was slightly too large⁶¹.

Calculated Density of States
at the Fermi Level E_F for
Nickel-Aluminum Alloys

ORIGINAL PAGE IS
OF POOR QUALITY



$N(E_F)$
States
eV(atom)

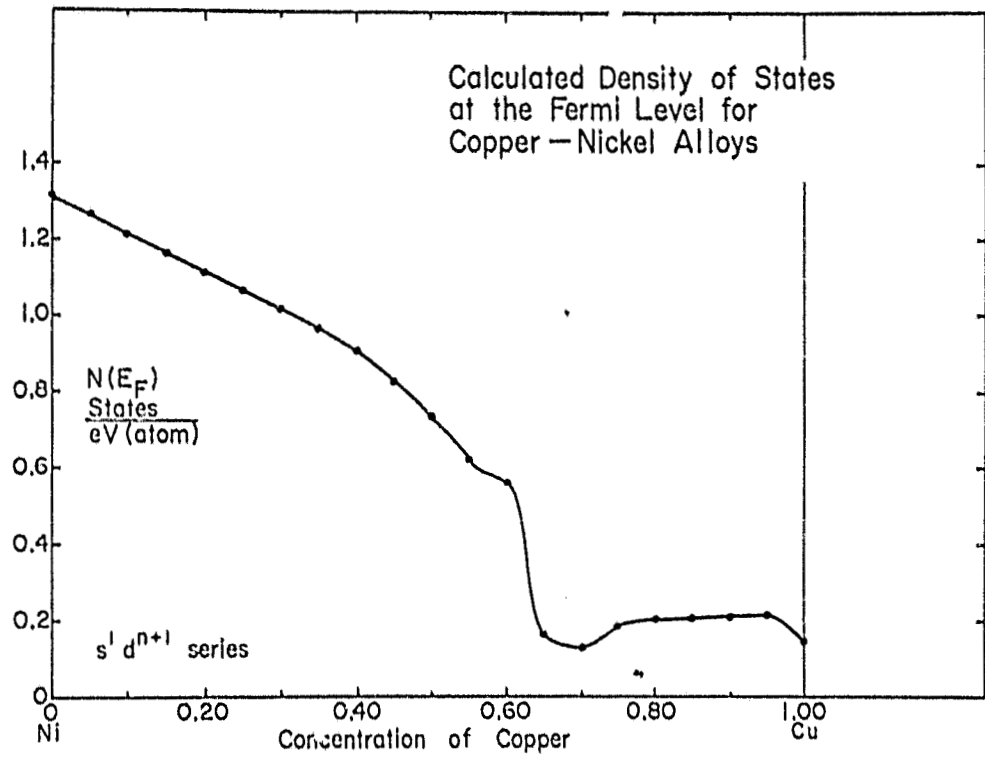
Concentration of Aluminum

1.00
Al

0
Ni

ORIGINAL PAGE IS
OF POOR QUALITY

Fig. 16.



Calculated Density of States
at the Fermi Level for
Titanium - Aluminum Alloys

ORIGINAL PAGE IS
OF POOR QUALITY

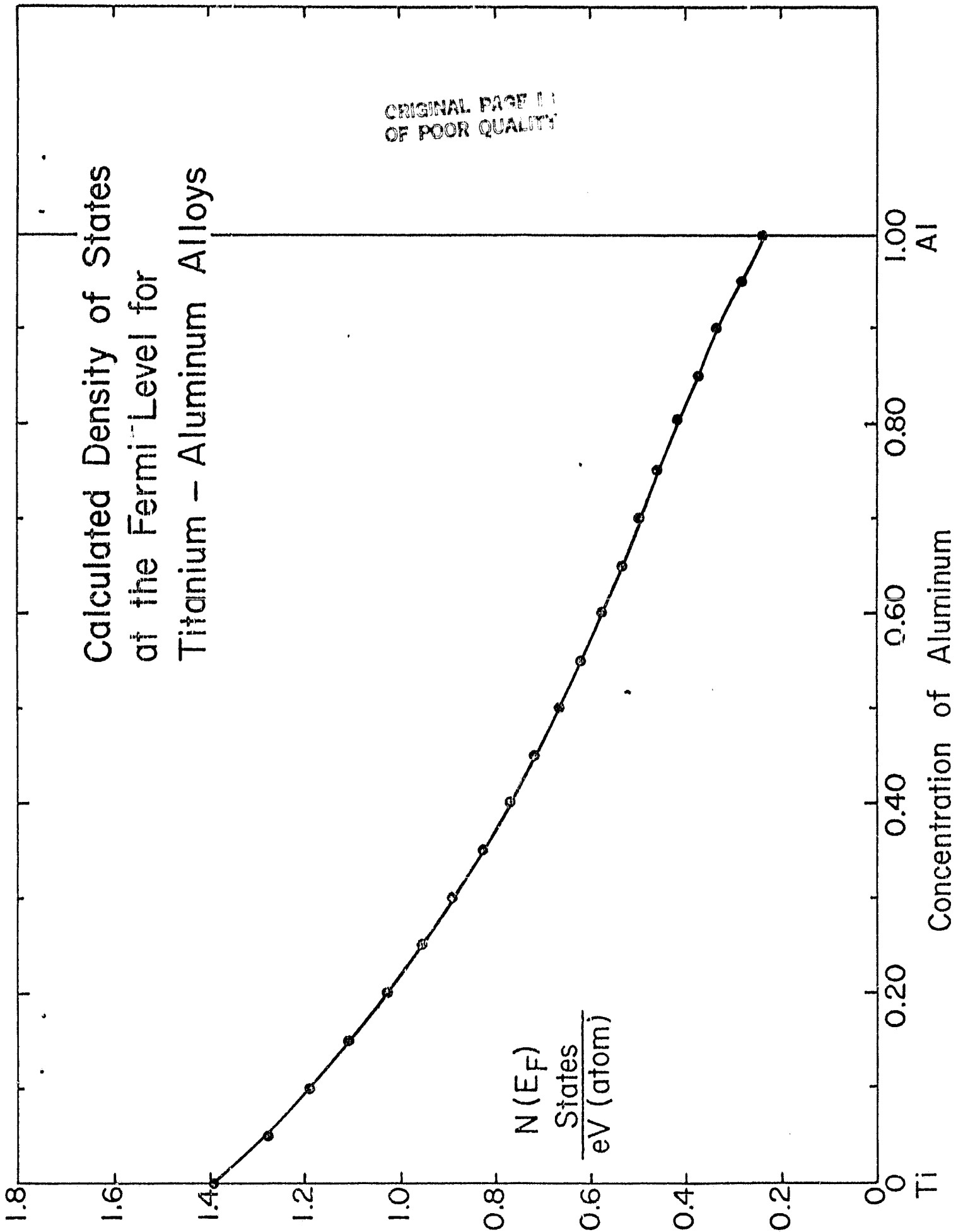
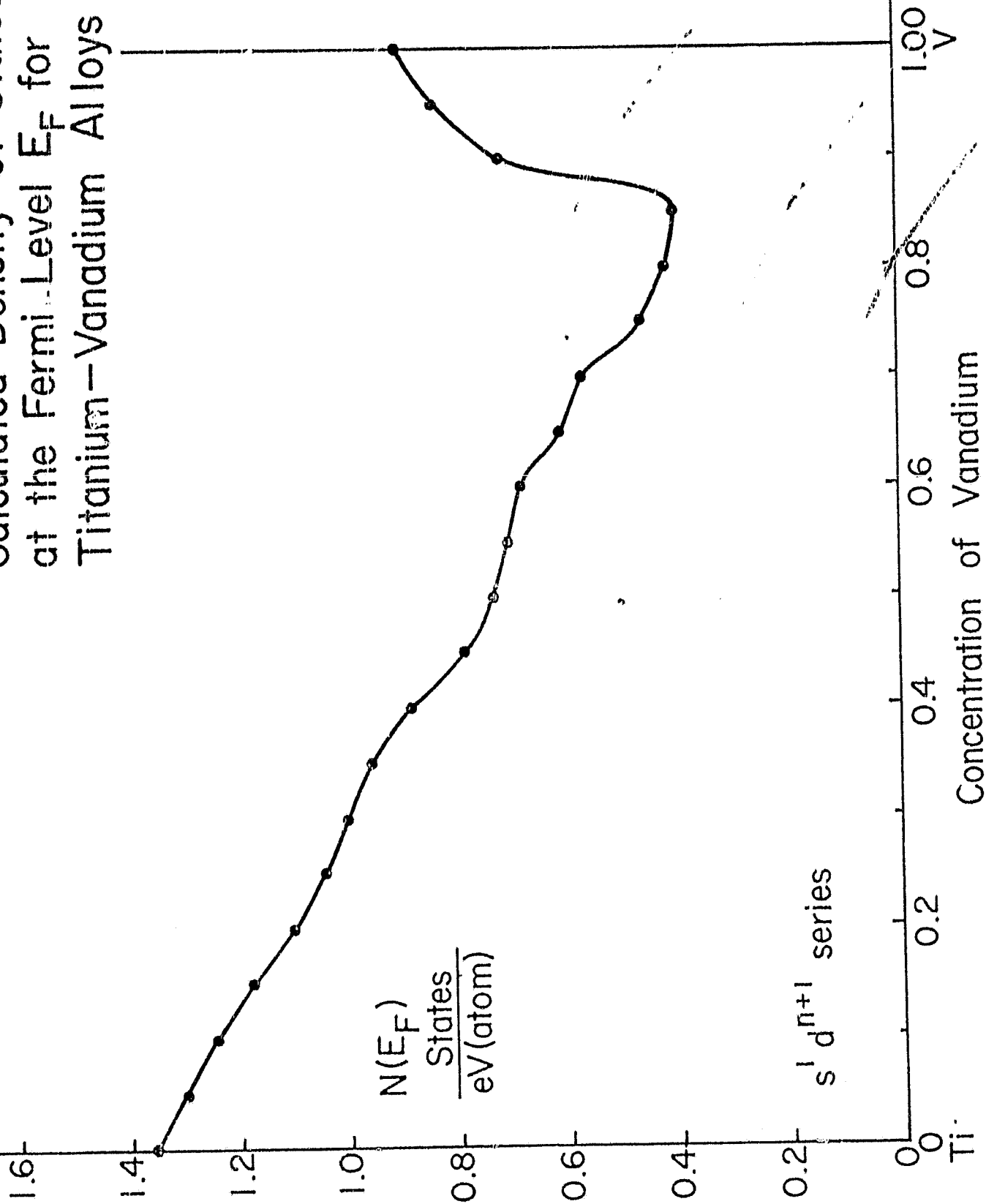


FIG. 18.

Calculated Density of States
at the Fermi-Level E_F for
Titanium-Vanadium Alloys



$s^1 d^{n+1}$ series

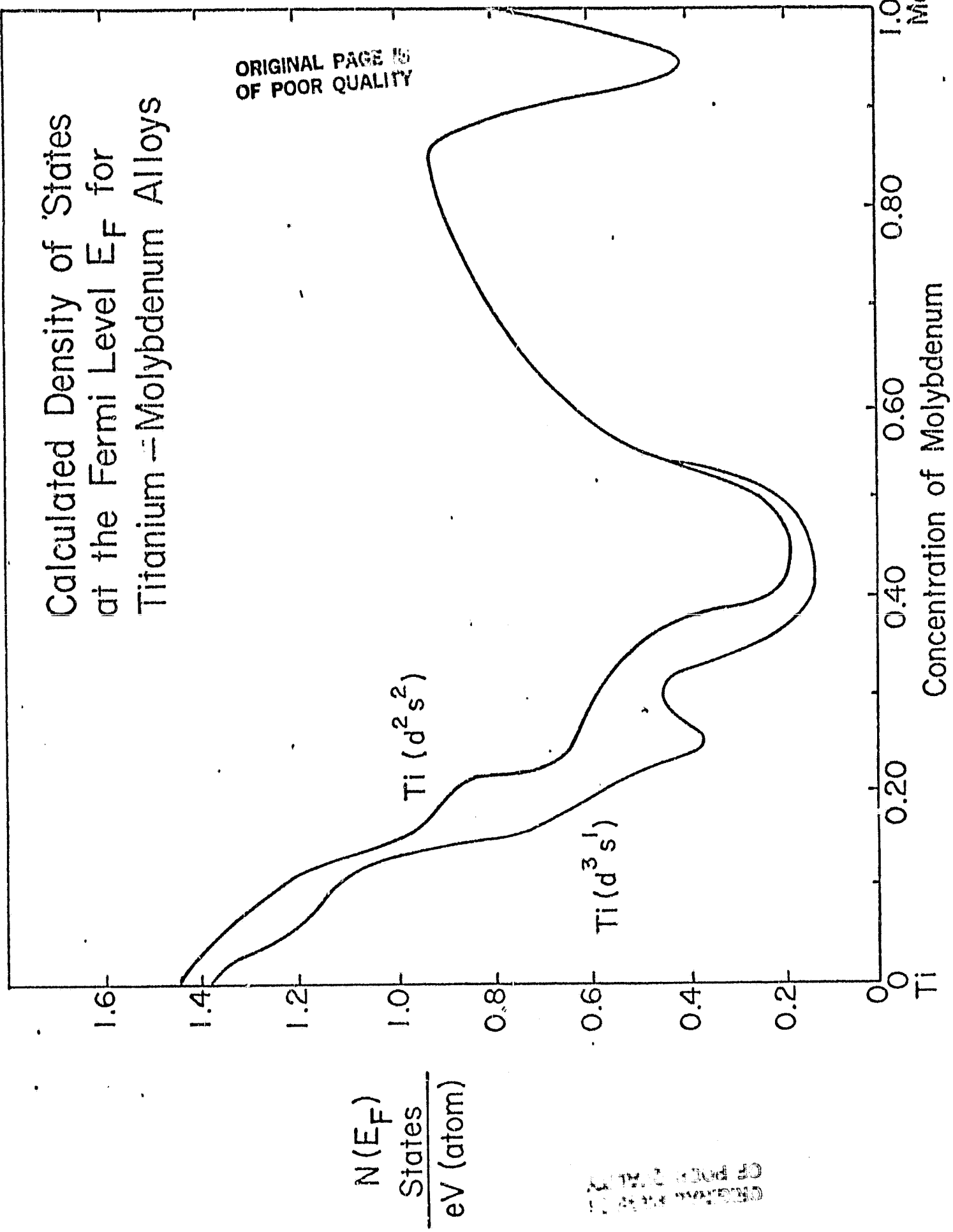
Ti

Concentration of Vanadium

1.00 V

Calculated Density of States at the Fermi Level E_F for Titanium - Molybdenum Alloys

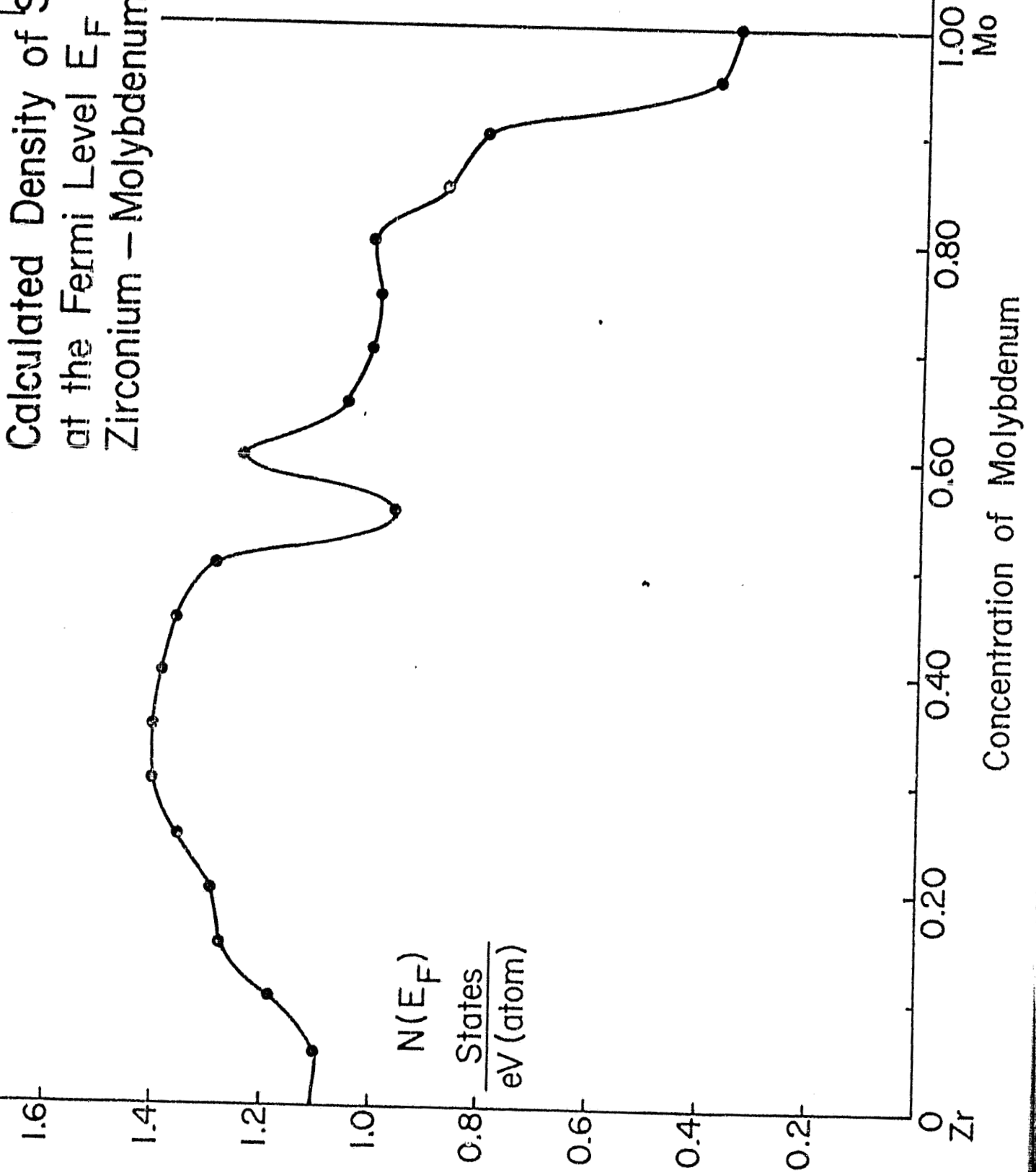
ORIGINAL PAGE IS OF POOR QUALITY



ORIGINAL PAGE IS OF POOR QUALITY

Calculated Density of States
at the Fermi Level E_F for
Zirconium - Molybdenum Alloys

ORIGINAL PAGE IS
OF POOR QUALITY



We investigated¹⁸ two typical alloy additions to iron, using the LCDS model--namely, chromium and manganese. The total alloy energies are shown for the two cases. The first, namely Fig. 21, shows that MN, a well known austenite former, will stabilize the γ phase at 0°K. The crossover point is surprisingly close to the value determined from the Fe-Mn phase diagram. In contrast, as Fig. 22 shows, no concentration of chromium will stabilize the gamma phase at 0°K.

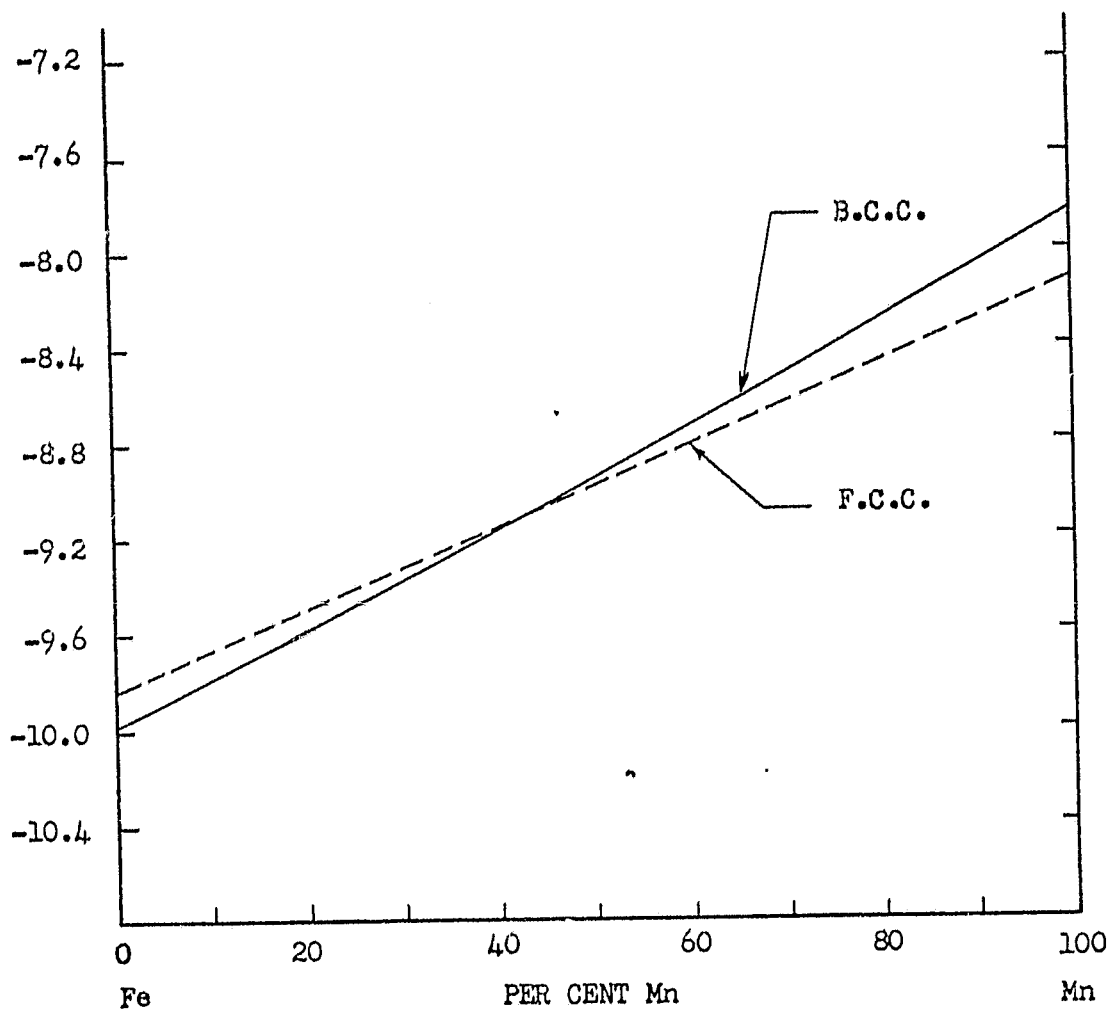
A logical extension of this work would be to study the effect of temperature on these two kinds of alloys. One defines formally the energy $E_F(T)$ the Fermi level for any temperature, as the energy at which the probability of a given energy state, being occupied is one-half--this is more general than the usual definition which only pertains to 0°K. Specifically, one would multiply the alloy $N(E)$ curve by the Fermi distribution function

$$f(E, T, E_F) = \left[1 + \exp \left(\frac{E - E_F(T)}{KT} \right) \right]^{-1} \quad (23)$$

to obtain the repopulation of the electronic levels in an alloy. With good luck, something approaching a phase diagram would be obtained.

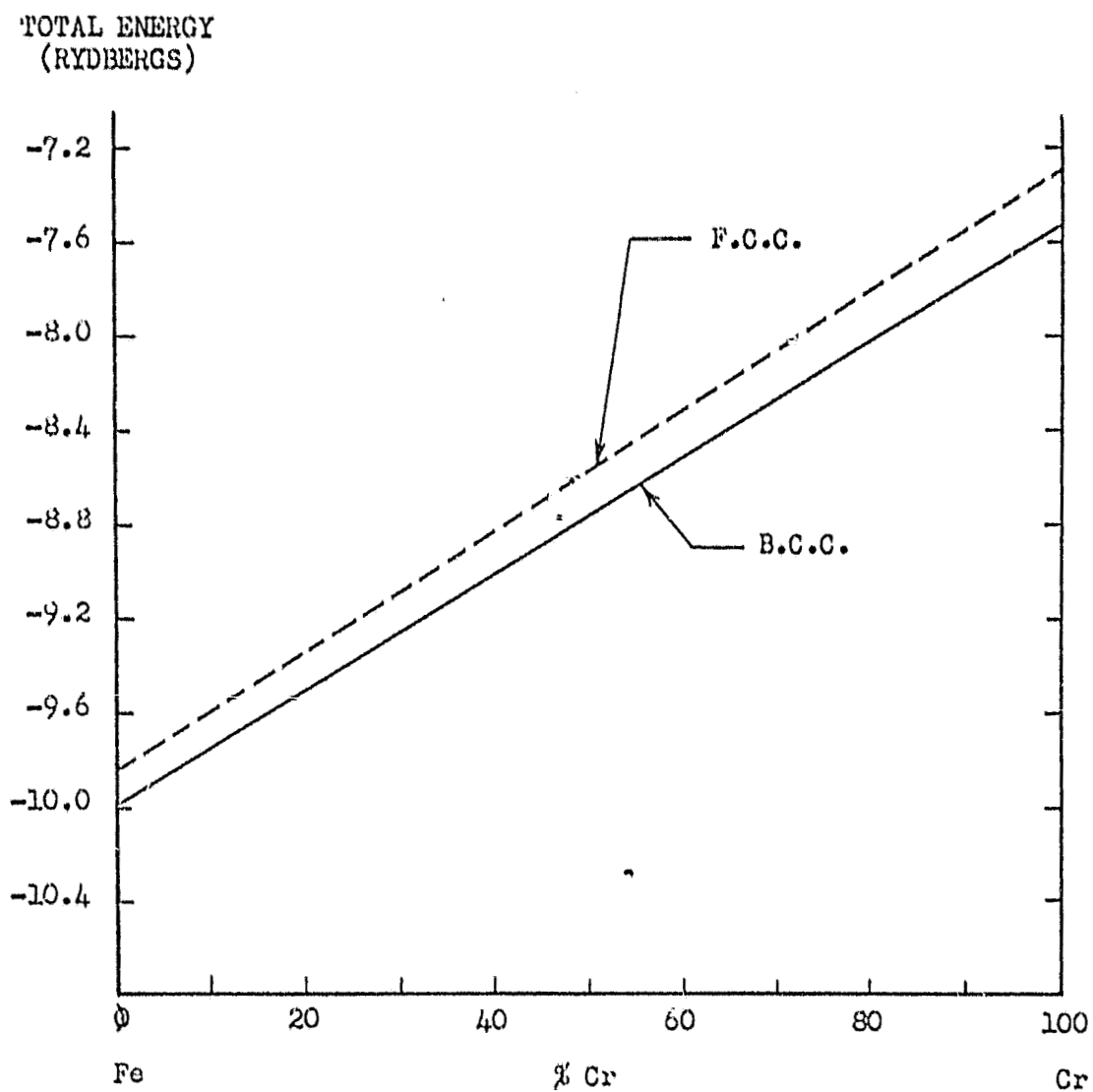
It is worthwhile to emphasize here that no thermodynamic facts have been built into the investigation. The atomic number and the interatomic distance are the only pieces of information fed into this to obtain individual density of states curves and the raw $N(E)$ curves in Fig. 23 were then combined to get the results just presented. Incidentally, the metals were "mixed" in the paramagnetic form and so the α - β Curie transformation was not used to bring about the change in stability of the α and γ phases⁶². Many refinements such as a better treatment of exchange, and the separate handling of spin up and spin down states, could be introduced. These would probably lead to an improved agreement with experimental results. It is, however, striking that the present simple treatments outlined above do lead to useful predictions and increased understanding.

TOTAL ENERGY
(RYDBERGS)



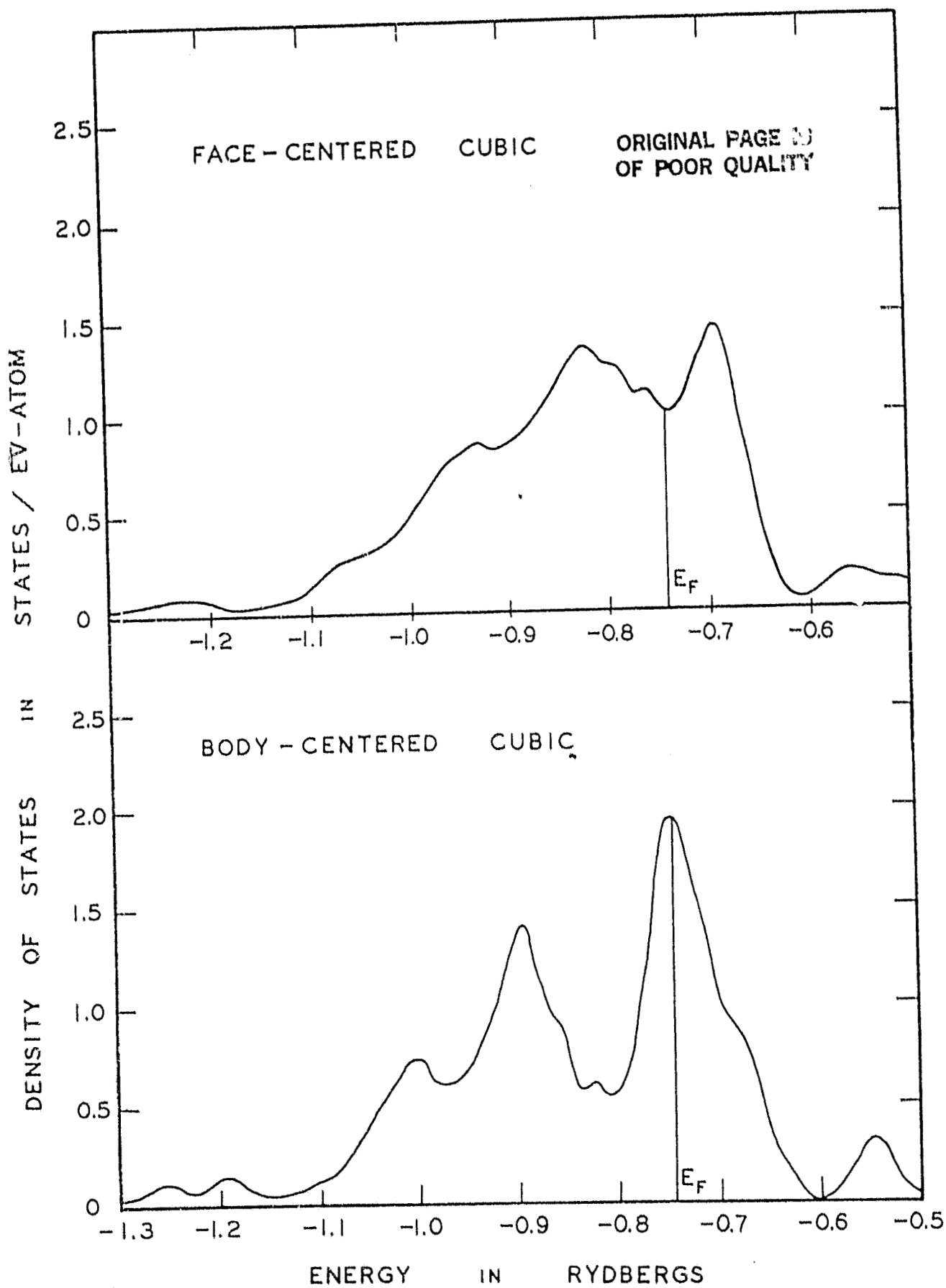
TOTAL ENERGY OF THE OCCUPIED ELECTRON STATES AT 0°K
AS A FUNCTION OF COMPOSITION FOR Fe ($3d^6 4s^2$) AND Mn ($3d^5 4s^2$)
ALLOYS.

Fig. 22.



TOTAL ENERGY OF THE OCCUPIED ELECTRON STATES AT
0°K FOR Fe ($3d^6 4s^2$) AND Cr ($3d^4 4s^2$) ALLOYS.

Fig. 23.



Hellman-Feynman Calculations

The Hellman Feynman theorem shows that the force F , acting on the p^{th} nucleus of a solid or molecule can be deduced (almost) classically from the total electronic charge density even though the latter is obtained from a quantum mechanical calculation. More specifically, the x component of F can be written as

$$F_{px} = Z_p \left[\sum_q \frac{Z_q}{(R_p - R_q)^2} \frac{\partial (R_p - R_q)}{\partial x_p} - \int \left(\frac{\rho(\mathbf{r}) x_p}{r_p^3} \right) d^3 r \right] \quad (24)$$

where Z_p is the charge on that nucleus, where x_p is the x component of \mathbf{r}_p and $\rho(\mathbf{r})$ is the total one electron density such as is found in a self-consistent calculation. That is, the force on the nucleus is the electrostatic force on a nucleus due to other nuclei and to the detailed distribution of surrounding electrons.

While this formulation is the adiabatic one, there have been dynamic treatments such as

$$M_p \ddot{x}_p = \left(\frac{\partial W_N}{\partial x_p} \right) - \int \rho(\mathbf{r}, t) \frac{\partial V}{\partial x_p} d^3 r \quad (25)$$

where W_N is the internuclear coulombic force and $\partial V / \partial x_p$ is the instantaneous force acting on the nucleus due to varying charge density $\rho(\mathbf{r}, t)$.

Debs⁶³ has made a very up-to-date review of the force concept deduced from the Hellman-Feynman theory. Slater⁶⁴ has rederived the theorem based on multiple scattering X α method he has used for deriving molecular wave functions. The promise of this Hellman-Feynman theory has been less than expected and the difficulty has been attributed to the poor quality of molecular wave functions which have been available.

This theory looks particularly useful for obtaining the relative movement and rearrangement of atoms at a free or on internal interface. It also appears to have a ready application to absorption of gaseous species on a metal.

Slater⁶⁴ pointed out that the equilibrium spacing of the surface nuclei will increase if there is an excess charge density on the side away from bulk; it will pull the nuclei out. In the contrary situation, it will decrease the interatomic distance. The vector sum of forces arising from the non-spherical electron distribution will give rise to a surface pressure.

In 1969, Wannier et al⁶⁵ calculated the force for lithium atoms at the surface. They found a large positive internal pressure which would have led to considerable dilation. After pointing out some errors in Wannier's treatment, Kleinman⁶⁶ showed that the forces on individual atoms will vanish if one assumes a slight increase of surface charge by 0.049e and with a slight outward movement of the nuclei in the surface plane by only 0.00395a₀. Without this dilation, Kleinman found a very substantial negative internal pressure redistribution near the surface.

DISCUSSION

Using an ionic model, Gilman⁶⁷ was able to show that the elastic compressibility modulus E of a series of AB compounds was proportional to the inverse fourth power of r_{AB} . When applied to metals, it was found that E depended on $r^{-\nu}$ where ν approached five.

The compressibility is properly obtained in the following manner

$$B = \frac{1}{k} = \nu \left(\frac{dR_s}{dV} \right)^2 \frac{d^2 E_T}{dR_s^2} = \frac{1}{12\pi R_s} \left(\frac{d^2 E_T}{dR_s^2} \right) \quad (26)$$

As an alternative procedure, one might consider calculating $\frac{dP}{dR_s}$ from Equation 12 which would lead to a term in dV/dR_s . However, this equation is already another form of

$$P = -N \left(\frac{dR_s}{dV} \right) \left(\frac{dE_T}{dR_s} \right) \quad (27)$$

In either form, one would obtain an expression involving R_s^{-1} before the second derivative, but the numerical factor would be significantly different.

One can readily compute the second derivative of E_T with respect to R_s . This is

$$\begin{aligned} \frac{d^2 E_T}{dR_s^2} = & \frac{4 \left[3NR_o^2 + 6\ell(\ell+1) \right]}{R_s^5} + \frac{3 \left[6\ell(\ell+1) - 4.42 a \right]}{R_s^4} \\ & + \frac{\left[3N - 1.2N - 0.916 a \right]}{R_s^2} + \frac{4b}{\rho_{BM}^2} \exp \left(- \frac{S_{ij}}{\rho_{BM}} \right) \end{aligned} \quad (28)$$

where a involves the cube root of N .

Thus, B can be written as

$$B = \frac{-12NR_0^2}{12\pi R_s^6} + \frac{24\ell(\ell+1)}{12\pi R_s^6} + \frac{18\ell(\ell+1) - 13.26a}{12\pi R_s^5} + \dots \quad (29)$$

since both R_s and R_0 are greater than unity, the lead terms become

$$B = \frac{N}{\pi} \left(\frac{R_0^2}{R_s^6} \right) + \frac{3\ell(\ell+1)}{2\pi R_s^5} \quad (30)$$

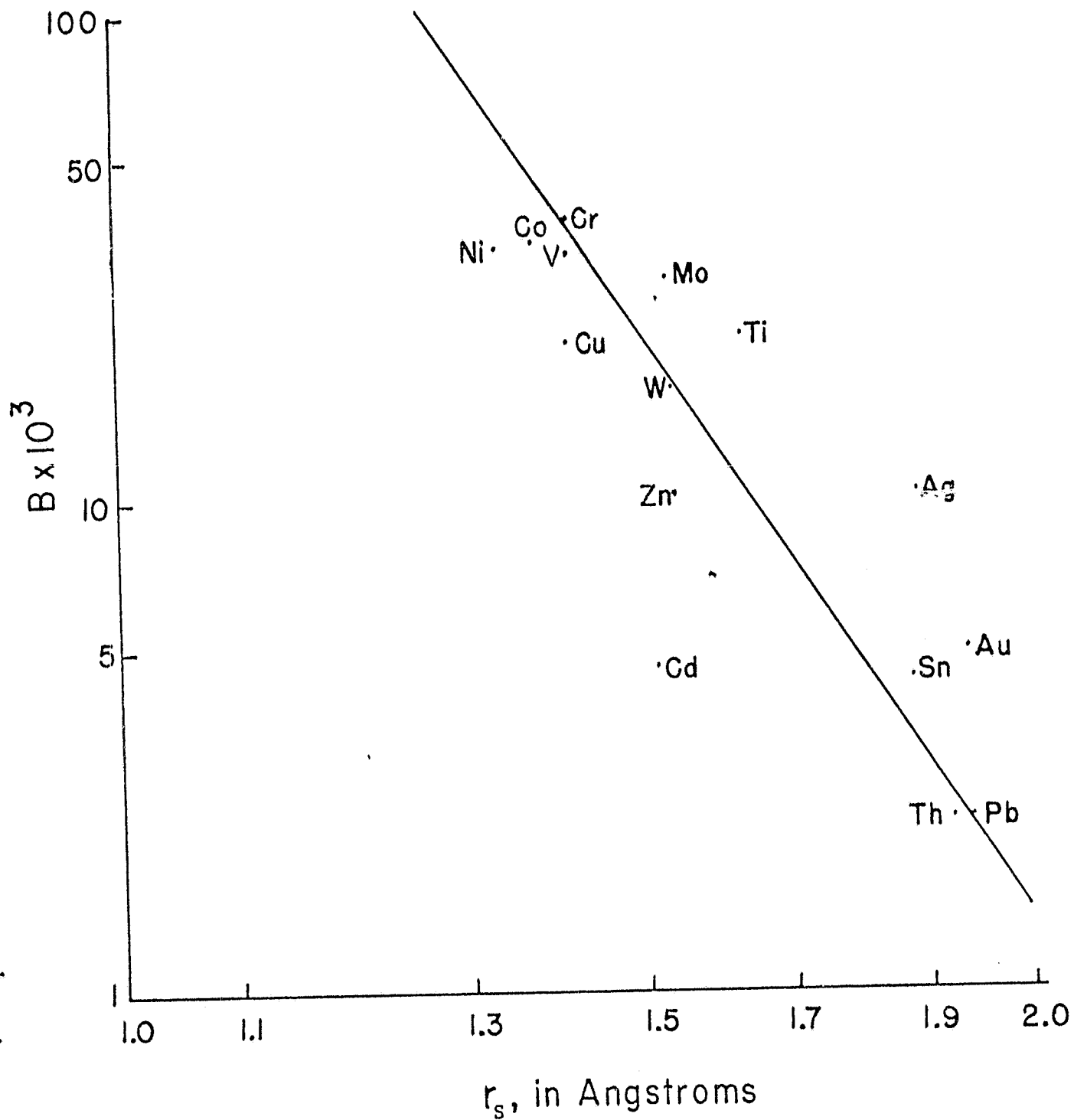
This deduction can be checked by using experimental values of B. The slope in Fig. 24 is for various transition metals and metals with differing valences and crystal structures is larger than 6. Subsequent plots given by Gilman⁶⁸ show that the slope is larger than 5 for transition metals. This is merely a further indication of the type of success which the volume-dependent FR model can be expected to yield.

One purpose of this paper is to emphasize how directly many of the properties of metals and alloys are tied to the pressure of the electronic gas which comes from the electrostatic repulsion between the electrons. Equilibrium distances, heats of formation as well as compressibility can readily be computed using slight modifications of the Fröhlich-Raimes model.

In the FR model, the kinetic energy term is computed as though the electrons were represented by a parabolic band, i.e. by a structureless $N(E)$ curve. But we know that such a description is inadequate per se. To offset this deficiency, we have incorporated a discussion of the use of the richly structured $N(E)$ curves for actual metals.

Let us turn to the LCDS model which is structure sensitive. The volume dependent effects are not included here, but they could readily be incorporated when sufficient data on the variation of the $E(k)$ curves as a function of R_s become available.

The Rigid Band model assumes that the Fermi level and hence the



$N(E+\beta H)$ and $N(E-\beta H)$ values at E_F , are readily calculated from (c/a) ratio without knowing partial spin bands of the constituents.

One successful aspect of the LCDS model is that it offers a simple logical reason for the deviations from the idealized Slater-Pauling curve of unpaired spins $N(E)$. For differing atomic numbers, the $N(E)$ curve may be very different in width and variable in location with respect to vacuum. The number of paired spins at E_F is thus not simply related to the density of states curve of either constituent since it depends on the response of the two partial spin up and two spin down bands in a binary alloy to the internal magnetic field βH . Even in a pure metal, $N(E_F \uparrow)$ is not equal to $N(E_F \downarrow)$ and hence transfer of electrons from one partial band to another occurs and leads to an unbalance in the pairing of spins. If the two constituents are elements of very different atomic number, the effect of a magnetic field on each $N(E)$ curve may be quite different while the effect of solute additions may result in recognizable trends in Slater-Pauling curves. There is no reason to anticipate that the height and the width of the individual alloy curves could be superimposed when plotted against (c/a) values.

R. E. Hummel et al⁶⁹, using differential reflectivity, observed that the adsorption edge (or change in the imaginary component ϵ_2 of the dielectric constant) associated with the d-bands of copper, did not move to lower energy with nickel additions. The energy separation between the peak energy did not move. They also measured the reflectivity of Cu-Zn alloys and noted that the energy separation between the d-bands and E_F does increase with Zn content. This they rationalize by making the energy of the state J_1 the same in pure Cu as in α -brass. Thus, the energy level E_F should increase with C_A due to the increase in the mean number of valence electrons. These observations on CuNi and CuZn alloys are not inconsistent with the LCDS model.

Other theoretical predictions for CuNi alloys have been made by

Lang and Ehrenreich⁷⁰ and by Stocks, Williams and Faulkner⁷¹. The former group predicts that $N(E_F^d)$ should decrease linearly with C_{Cu} whereas the Oak Ridge group which used the CPA approach predict a more rapid initial decrease followed by a leveling off above 60 per cent copper. It is interesting to note that Huffner et al⁷² point out that their experimental density of states for the alloys "...to a very good approximation, be made up by superimposing those of Ni and Cu."

To date, no synthesis of these distinct approaches has been attempted. Pragmatically, they are two limiting cases of the more complex true situation. While my colleagues and I are working on such a synthesis, it is hoped that this review will stimulate some readers to undertake the overall problem, and make a significant contribution to the science of metals.

Acknowledgement

The author would like to thank Dr. Allen C. Larson (Los Alamos Scientific Laboratory) who was of considerable help when this idea was first investigated and to Mr. F. W. Schonfeld and Prof. K. Gschneidner who offered continuing encouragement over the intervening years. Because of these three individuals, a summary is at last been made available.

The LCDS model arose from discussions with John Wood and A. C. Switendick. Exploration of the model can be attributed to the intensive work of David Koskimaki while he was a graduate student in the Materials Science Department of Northwestern University.

To these individuals in particular and to numerous colleagues who have offered guidance and criticism, the author acknowledges his indebtedness and apologizes for not citing each of them.

Table of Captions

- Fig. 1. Plot illustrating the dependence of R_0 on the ionization potential w^2 and on the valence N . The continuous curve is band $N=4$. Waber and Larson used r_0 in place of R_0 . Their Eq. (7) corresponds to Eq. (6) herein and their Eq. (5) is obtained by setting $A=0$.
- Fig. 2. Plot of the different electron-electron interaction terms in Eq. (9) (after Larson and Waber⁷).
- Fig. 3. Determination of K_0 and ρ from E_0 and E_T curves of titanium and zirconium.
- Fig. 4. The calculated pressure dependence of χ for four different tetravalent metals.
- Fig. 5. Comparison of experimental shock wave data of McQueen and Marsh⁴¹ for nickel with two calculated P versus V curves. The higher valence $N=3$ (which is chemically stable) is an approximate way of taking account of repulsion between d-electrons and ion-cores.
- Fig. 6. Similar Shock-Wave data for gold compared with those calculated from $E_T(R_s)$ with and without E_{ionic} from Eq. (14) included.
- Fig. 7. Plot of $-E_L(C_A, \rho)$ evaluated at the composition dependent radius $\rho(C_A)$ for titanium-cerium alloys. The effect of assuming that cerium is tetravalent is to cause only a slight depression in the E_T curve. It is interesting that $\rho(C_A)$ lies above the straight line connecting the ρ values for the two pure materials. A positive deviation is indicated from Vegard's Law of additive atomic radii.
- Fig. 8. Similar plot for sodium-silver alloys which indicates a large positive deviation from Vegard's Law.
- Fig. 9. The strong negative deviation from Vegard's Law for sodium-magnesium alloys contrasts with the alloys curves presented so far.

Table of Captions (cont.)

- Fig. 10. Experimental values of the two lattice parameters of a series of hexagonal metals. In the middle of the composition range, titanium-zirconium alloys become body-centered cubic at room temperature according to Duwez⁴³.
- Fig. 11. Plot of $-E_c(C_A)$ and $\rho(C_A)$ for titanium-zirconium alloys.
- Fig. 12. Variation of the pressure volume curves calculated for titanium-zirconium alloys.
- Fig. 13. $N(E)$ curves for pure copper and nickel obtained by Waber and Snow¹⁴ using Slater's exchange parameter $\chi\alpha=1$. These two curves are combined to obtain Fig. 14.
- Fig. 14. Set of density of states $N(E_F^a)$, curves calculated for several nickel-copper alloys using the LCDS model of Koskimaki and Waber¹⁸.
- Fig. 15. Composition dependent change in the density of states $N(E_F^a)$ at the calculated Fermi level E_F^a for homogeneous nickel-aluminum alloys.
- Fig. 16. A similar plot of the variation of $N(E_F^a)$ for homogeneous nickel-copper alloys. The individual Fermi levels are not shown in Fig. 14.
- Fig. 17. Composition dependent density of states at the Fermi level E_F^a calculated for homogeneous titanium-aluminum alloys.
- Fig. 18. Similar plot of $N(E_F^a)$ for titanium-vanadium alloys.
- Fig. 19. Similar plot of $N(E_F^a)$ for titanium-molybdenum alloys. Separate curves are given for the configurations d^2s^2 and d^3s assumed for BCC titanium by Waber and Snow¹⁴.
- Fig. 20. Similar plot for homogeneous zirconium-molybdenum alloys.
- Fig. 21. Total energy of occupied electron states at 0°K as a function of composition using bands calculated for both pure phases with iron ($3d^64s^2$) and manganese ($3d^54s^2$). The transformation from FCC to BCC as manganese is added is indicated.

Table of Captions (cont.)

- Fig. 22. A similar plot which shows that no chromium addition is sufficient to stabilize the austenite at 0°K. Based on data calculated by Snow and Waber¹⁴ using chromium with the $3d^4 4s^2$ input configuration.
- Fig. 23. Comparison of the density of states curves for FCC and BCC iron in a paramagnetic state. Note the difference in height and slope at E_F . (after Snow and Waber¹⁴)
- Fig. 24. Log-log plot of experimental values of the bulk modulus against the cell radius r_s (in Angstroms). Slope of the line is larger than 6.

REFERENCES

1. H. Brooks: Nuovo Cimento, 1958, vol. 7, supplement 2, pp. 166-244.
2. E. P. Wigner and F. Seitz: Solid State Physics, 1955, vol. 1, pp. 97-126.
3. H. Fröhlich: Proc. Roy. Soc., 1937, vol. A158, pp. 97-110.
4. S. Raimes: Phil. Mag., 1952, ser. 7, vol. 43, pp. 327-337.
5. S. Raimes: Proc. Phys. Soc., 1953, vol. A66, pp. 949-950.
6. B. T. Bernstein: Iowa State Univ., thesis, 1959, Univ. Microfilms, Inc., Ann Arbor, Mich., No. Mic. 60-568, p. 120.
7. A. C. Larson and J. T. Waber: Bull. Am. Phys. Soc., 1963, vol. 8, p. 10.
8. A. C. Larson, J. T. Waber and J. F. Smith: Los Alamos Scientific Lab and Iowa State Univ., unpublished research, 1964.
9. H. E. Jones: Proc. Roy. Soc., 1934, vol. A144, p. 225; 1934, vol. A147, p. 396; Proc. Phys. Soc., 1937, vol. A49, p. 250; Phil. Mag., 1952, vol. 43, p. 105.
10. W. Hume-Rothery: A review is given in Hume-Rothery, R. Smallman and C. W. Hayworth: Structure of Alloys, Institute of Metals, London, 1969.
11. J. C. Slater: Phys. Rev., 1936, vol. 55, p. 675.
12. An example of the Slater-Pauling curve is given in P. Crangle in P. Beck, ed.: Electronic Structure and Alloy Chemistry of the Transition Elements, p. 57, Interscience, New York, 1963.
13. S. Raimes: J. Phys. and Rad., 1962, vol. 23, p. 63°
14. E. C. Snow and J. T. Waber: Acta Met., 1969, vol. 17, p. 64.
15. M. F. Manning: Phys. Rev., 1943, vol. 63, p. 190. J. B. Greene and M. F. Manning: Ibid., p. 203.
16. M. Chodorow: Phys. Rev., 1939, vol. 55, p. 675. See also H. M. Krutter: Phys. Rev., 1935, vol. 48, p. 664; and K. Fuchs: Proc. Roy. Soc., 1935, vol. A151, p. 585.

17. J. T. Waber, see discussions in L. H. Bennett, ed.: Electronic Density of States, Special Publ. 323, pp. 221, 323, 817, Nat. Bur. Stand, 1971.
18. D. Koskimaki and J. T. Waber: Northwestern Univ., unpublished research, 1971.
19. E. W. Collings and H. Gegel: This Conference.
20. E. Sterns: Phys. Rev., 1972, vol. B5, p. 368.
21. S. B. Trickey, F. W. Averill, and F. R. Greene, Jr.: Phys. Lettr., 1972, vol. 9, p. 385.
22. F. Perrot: Theses d'etat, Paris, 1971.
23. E. C. Snow: "Total Energy as a Function of Lattice Parameter for Copper via the Self-Consistent APW Method," submitted to Phys. Rev. Also "Compressibility of Copper via the Self-Consistent APW Method," submitted to Solid State Comm.
24. We have followed the traditional Wigner-Seitz boundary condition. However, the correct one is ℓ -dependent and the gradient vanishes for even values of ℓ , but it is necessary for the wave function to vanish at R_s for ℓ odd to insure the proper matching of wave functions in contiguous cells.
25. Even though the right-hand side of Eq. 4a may become negative, the term $\beta R_0 \cot \beta R_0$ remains real since the $\sin(ix) = i \sin \lambda x$ and $\cos(ix) = \cos \lambda x$. The logarithmic derivative in Eq. 6, however, becomes a complex number unless A is set equal to zero.
26. J. C. Slater: Phys. Rev., 1951, vol. 81, p. 385; Adv. Quant. Chem., 1972, vol. 6, p. 1. K. Schwarz: Phys. Rev., 1972, vol. B5, p. 2466. J. C. Slater and K. H. Johnson: Phys. Rev., 1972, vol. B5, p. 844. L. Hedin and S. Lundquist: J. Phys. Colloq., 1972, vol. C3, p. C3-7.
27. D. Liberman: Phys. Rev., 1971, vol. B3, p. 2081.
28. D. Pines and P. Nozières: Phys. Rev., 1958, vol. 111, p. 442.

29. K. Gschneidner: Rare Earth Alloys, p. 25, Van Nostrand, New York, 1961.
30. O. C. Trulson, D. E. Hudson and F. H. Spedding, Jr.: Jour. Chem. Phys., 1961, vol. 35, p. 1018.
31. P. Bridgman: The Physics of High Pressure, pp. 160-161, Strageways Press, London, 1952.
32. G. L. Pearson and W. H. Brattain: Proc. Inst. Radio Eng., 1955, vol. 43, pp. 1794-1806.
33. G. Teatum, K. Gschneidner and J. Waber: Los Alamos Scientific Laboratory Document LA 2345, June 1960, 235 p., revised 1970.
34. C. E. Moore-Sitterly: Nat. Bur. Stand., 1949, Circular 467, vols. I, II and III.
35. W. Finkelburg and W. Humbock: Naturw., 1955, vol. 42, p. 35. See also Phys. Rev., 1950, vol. 77, pp. 303-304.
36. P. F. A. Klinkenberg, A. M. van Kleef and P. E. Noorman: Physica, 1961, vol. 27, p. 151.
37. S. Raimes: Imperial College, New York, unpublished research, 1951.
38. J. T. Waber and A. C. Larson: Rare Earth Research II, pp. 351-383, Gordon & Breach, New York, 1964.
39. H. Brooks: Trans. TMS-AIME, 1963, vol. 227, p. 546.
40. T. S. Kuhn: Phys. Rev., 1950, vol. 79, p. 515.
41. S. McQueen and S. P. Marsh: Jour. Appl. Phys., 1960, vol. 31, p. 1253. The Hugoniot is a pressure volume based curve which allows for significant temperature rise, and is based on the Hugoniot-Rankine Equations. The curve marked isentrope, allows for the reduction of temperature to 0°K isentropically.
42. D. Hafemeister and J. Zahrt: Jour. Chem. Phys., 1967, vol. 47, p. 1629. See also D. Hafemeister: Jour. Chem. Phys., 1965, vol. 43, p. 789.

43. W. B. Pearson: A Handbook of Lattice Spacings and Structures of Metals and Alloys, pp. 876-878, Pergamon Press, New York, 1958.
44. J. T. Waber, I. R. Harris and G. V. Raynor: Trans. Amer. Inst. Met. Eng., 1964, vol. 230, p. 148.
45. J. J. Friedel: Phil. Mag., vol. 46, ser. 7, p. 514.
46. K. Gschneidner and F. J. Vineyard: Jour. Appl. Phys., 1962, vol. 33, p. 3444.
47. J. R. Harris and G. V. Raynor: University of Birmingham, private communication, 1961.
48. J. E. Davison and J. F. Smith: Trans. TMS/AIME, 1968, vol. 242, p. 2045.
49. G. W. Shannetti and J. F. Smith: Jour. Appl. Phys., 1971, vol. 42, p. 2799. A. Samer and J. F. Smith: Jour. Appl. Phys., 1962, vol. 33, p. 2283.
50. P. Bolsaitis: Met. Trans., 1973, vol. 4, pp. 2395-2398.
51. R. Chiarodo, J. Green, I. L. Spain and P. Bolsaitis: Jour. Phys. Chem. Solids, 1972, vol. 33, pp. 1905-1914.
52. K. Hsieh and P. Bolsaitis: Jour. Phys. Chem. Solids, 1972, vol. 33, pp. 1838-1842.
53. R. T. Sanderson: Chemical Periodicity, p. 25, Reinhold Publ. Co., New York, 1960.
54. K. H. Johnson in L. H. Bennett and J. T. Waber, eds.: Energy Bands in Metals and Alloys, p.108, Gordon and Breach, New York, 1968. K.H.
55. Johnson and J. W. D. Connolly: Int. Jour. Quant. Chem., 1970, vol. III, p. 813.
56. P. Soven: Phys. Rev., 1967, p. 809. See also Fig. 1 of article by Soven in L. H. Bennett and J. T. Waber, eds.: Energy Bands in Metals and Alloys, p. 146, Gordon and Breach, New York, 1968.
57. For example, see D. E. Eastman, J. K. Cashman and A. C. Switendick: Report RC 5368, I.B.M..Co., 1971. D. E. Eastman:

57. (cont.) Proc. Conference on Electron Spectroscopy, Asilmoar, 1971.
For pure metals, see D. E. Eastman: Jour. Appl. Phys., 1969,
vol. 40, p. 1387; and J. F. Janak, D. E. Eastman and A. R.
Williams: Solid State Comm., 1970, vol. 8, p. 271.
58. D. H. Seib and W. E. Spicer: Phys. Rev. Lett., 1968, vol.
20, p. 1441; also, Phys. Rev., 1970, vol. B2, pp. 1676 and
1694; W. E. Spicer: Phys. Rev., 1967, vol. 154, p. 385;
C. N. Berglund and W. E. Spicer: Phys. Rev., 1964, vol. 136,
pp. A1030 and A1044.
59. J. Clift, C. Curry and B. J. Thompson: Phil. Mag., 1963, vol.
8, p. 592.
60. L. H. Bennett and R. Willens, eds.: Charge Transfer/Electronic
Structure of Alloys, Met. Soc. of the Am. Inst. of Mining, Met.
and Pet. Eng., New York, 1974.
61. D. Koskimaki and J. T. Waber in L. H. Bennett, ed.: Elect-
ronic Density of States, p. 741, Spec. Publ., Nat. Bur. Stand.,
1971.
62. Investigation of temperature effects in repopulating various
states was investigated; just using the quantum statistics, it
was shown that γ Fe becomes more stable with increasing
temperature but Fe converts back to the B.E.C. δ -Fe at sufficiently
high temperatures, due to electron-phonon interaction effects.
63. B. M. Deb: Rev. Mod. Phys., 1973, vol. 45, pp. 22-43.
64. J. C. Slater: Jour. Chem. Phys., 1973, vol. 57, p. 2389.
65. G. H. Wannier, C. Misner and G. Schay: Phys. Rev., 1969, vol.
185, p. 983.
66. L. Kleinman: Phys. Rev., 1971, vol. B3, p. 3083.
67. J. J. Gilman: Nat. Bur. Stand. Monograph, 1963, no. 59, pp.
79-102.
68. J. J. Gilman in J. E. Burke, ed.: Progress in Ceramic Science,
pp. 146-199, Pergamon Press, New York, 1961.

ORIGINAL PAGE IS
OF POOR QUALITY

69. R. E. Hummel, J. A. Holbrook and J. B. Andrews: Surface Science, 1973, vol. 37, p. 717.
70. N.D. Lang and H. Ehrenreich: Phys. Rev., 1966, vol. 152, p. 520.
71. G. M. Stocks, R. W. Williams and J. S. Faulkner: Phys. Rev. Lettr., 1971, vol. 26, p. 354; see also Phys. Rev., 1971, vol. B4, p. 4390.
72. G. Ruffner, G. K. Wertheim, R. L. Cohen and J. H. Wernick: Phys. Rev. Lettr., 1972, vol. 28, p. 438.